Accepted manuscript doi:
10.1680/jgeot.22.00041

Accepted manuscript doi:
10.1680/jgeot.22.00041

Submitted: 01 February 2022

Published online in 'accepted manuscript' format: 10 February 2023

Manuscript title: The axial behaviour of piles driven in chalk

Authors: Richard J. Jardine*, Róisín M. Buckley[†], Tingfa Liu[‡], Thomas Andolfsson[§], Byron W. Byrne[‖], Stavroula Kontoe[¶], Ross A. McAdam**, Fabian Schranz[††] and Ken Vinck*

Affiliations: *Department of Civil and Environmental Engineering, Imperial College London, London, UK; [†]School of Engineering, Glasgow, UK; [‡]Department of Civil Engineering, University of Bristol, Bristol, UK; formerly Department of Civil and Environmental Engineering, Imperial College London, London, UK; [§]R&D engineer, SKB AB, Swedish Nuclear Fuel and Waste Management Co, Sweden; formerly Department of Engineering Science, Oxford University, Oxford, UK; [‖]Department of Engineering Science, Oxford University, Oxford, UK; [¶]Department of Civil Engineering, University of Patras, Patras, Greece; Imperial College London, London, UK; [**]Orsted Power (UK) Ltd., London, UK; formerly Department of Engineering Science, University of Oxford, Oxford, UK and [††]Office of the Tyrolean Regional Government, Innsbruck, Austria; formerly Department of Engineering Science, Oxford University, Oxford, UK

Corresponding author: Tingfa Liu, Department of Civil Engineering, University of Bristol, Queen's Building, BS8 1TR, Bristol, UK.

E-mail: tingfa-liu@hotmail.com

Accepted manuscript doi:
10.1680/jgeot.22.00041

Abstract

This paper describes research into the poorly understood axial behaviour of piles driven in chalk. Comprehensive dynamic and monotonic axial testing on 27, mostly instrumented, piles undertaken for the ALPACA Joint Industry Projects is reported and interpreted covering: diameters between 139mm and 1.8m; lengths from 3 to 18m; different pile material types; tip and groundwater conditions, and ages after driving. The experiments show the factors that influence resistance most strongly are: (i) pile end-conditions, (ii) slenderness ratio and flexibility, (iii) shaft material, (iv) age after driving, (vi) relative water table depth, and (vii) whether loading is compressive or tensile. Varying the factors systematically identified a remarkable average long-term shaft resistance range from below 11 kPa to more than 200 kPa for piles driven at the same low-to-medium density chalk test site in Kent (UK). Dynamic and static analyses demonstrate that soil resistances to driving (SRD) were generally well-predicted by the Chalk ICP-18 short-term formulation. Considering the piles' long-term behaviour, the Chalk ICP-18 approach over-predicted capacity, while the widely used CIRIA approach proved over-conservative for most cases. The research enabled the development of a revised 'ALPACA-SNW' long-term capacity assessment method that matches the test outcomes far more faithfully.

Keywords: Driven pile; chalk; axial capacity

Accepted manuscript doi:
10.1680/jgeot.22.00041

INTRODUCTION

Jardine et al. (2018, 2019) review the considerable uncertainty that exists regarding the behaviour of piles driven in chalk and describe the design of the ALPACA (Axial-Lateral Pile Analysis for Chalk Applying multi-scale field and laboratory testing) and ALPACA-Plus Joint Industry Projects (JIPs) to address shortfalls in current knowledge. This paper describes how the two JIPs identified the key factors that control the dynamic and monotonic, short-and-long term, axial behaviour of a wide range of driven piles and sets out an improved design approach. Buckley et al. (2022) report on the ALPACA studies into cyclic axial loading behaviour, while ALPACA AWG (2022) describe the JIPs' parallel investigations into monotonic and cyclic lateral loading.

BACKGROUND

Chalk occurs worldwide as a very weak to weak biomicrite limestone, composed of lightly cemented silt-sized $CaCO_3$ particles (Mortimore, 2013) and is encountered frequently at foundation depth in NW Europe. Conventional design rules have proved critically unable to predict adequately the behaviour of piles driven to support North and Baltic Sea offshore wind-turbines (Barbosa et al., 2017; Carotenuto et al., 2018; Buckley et al., 2020a). Refusals have occurred in high-density chalks, while piles have 'run' under self-weight to far greater-than-expected depths at low-medium density sites. Local de-structuration generates thin "putty" chalk annuli around open-ended piles with undrained shear strength S_u <10 kPa during driving (Hobbs & Atkinson, 1993; Buckley et al., 2018a; Vinck, 2021), which correlate with high natural liquidity indices. Doughty et al. (2018) and Vinck (2021) show that dynamic compaction of low-to-medium density chalk at natural water contents leads to similarly weak putties. Axial capacity growth, or set-up, develops after driving and Lord et al. (2002) recommend 120kPa ultimate shaft shear resistances in high density chalk and 20kPa for other grades, reducing to 10kPa for piles with slender shafts that experience marked transient elastic lateral displacements, or "whip", under driving. Loading tests reported by Barbosa et al. (2017) and Vinck (2021) proved far higher-than-predicted capacities, emphasising the need for more economical and reliable design methods.

Buckley et al. (2018b) and Buckley et al. (2020a) demonstrate that piles driven in chalk share several of the fundamental features captured in the ICP-05 (Jardine et al., 2005) design approaches for sands and clays:

- Base resistances q_b and local shaft radial effective stresses σ'_r and shear resistances τ_{rz} correlate linearly with local CPT tip resistance q_t.
- Local σ'_{rf} and τ_{rzf} reduce sharply as relative pile tip depth h (normalised by $R^* = (R^2_{outer} - R^2_{inner})^{0.5}$ grows during driving.
- Axial capacities vary markedly with time after installation, with long-term shaft resistances remaining affected by h/R* and local failure being governed by a Coulomb law with $\tau_{rzf} = \sigma'_{rf} \times \tan(\delta')$.
- Laboratory interface ring-shear tests provide accurate operational δ' angles $\approx 31^o$ to 32^o.

Buckley (2018) concluded that σ'_{rf} also varies with pile diameter-to-wall thickness ratio D/t_w during driving. Working with a sparse set of un-instrumented tension and dynamic tests on open tubular-steel piles driven at St Nicholas at Wade (SNW) in the UK and the Wikinger Baltic Sea windfarm, Jardine et al (2018) and Buckley et al (2020) proposed Chalk 'ICP-18' approaches for SRD and long-term capacity. A tension-to-compression shaft capacity ratio of unity was assumed, as found with clays, although a ratio ≈0.75 applies in sands due principal stress axis rotation effects, Jardine et al (2005)

Accepted manuscript doi:
10.1680/jgeot.22.00041

and 'Poisson' straining of pile shafts (De Nicola & Randolph 1993). However, analysis of other tests on large tubular steel piles driven at French and German chalk sites by Vinck (2021) and Vinck et al., (2023) indicated a lower ratio ≈0.5, including cases where the pile's internal plug had been removed by coring.

Implicit in Chalk ICP-18 is marked post-installation set-up. Buckley (2018) interpreted ageing trends from multiple monotonic tension tests on small piles driven (above the water table) at SNW and compressive Beginning-of-Restriking (BoR) capacities established from dynamically instrumented large piles driven offshore at the Wikinger Baltic windfarm site. Buckley (2018) normalised these capacities by compressive End-of-Driving (EoD) SRDs obtained by signal matching of instrumented dynamic records. Ciavaglia et al. (2017) noted similar trends from tension tests on other piles driven (above the water table) at SNW. Buckley et al. (2018a)'s interpretation of the onshore SNW tension tests' slow initial capacity growth, followed by marked gains over the subsequent months, did not recognise that the tension shaft capacities could be considerably lower than those available at the same age in compression. The like-for-like offshore EoD and BoR trends from Wikinger indicated final set-up ratios that reduced with h/R* and progressed more rapidly offshore than at SNW (see Buckley et al. (2020a)).

RESEARCH AIMS

The ALPACA and ALPACA Plus Joint Industry Projects (JIPs) aimed to develop reliable, fundamentally based, practical design approaches. As set out by Jardine et al. (2019), multi-scale field experiments were conducted on forty-one piles driven at SNW shown in Figure 1(a), with their heights, diameters and relative position to the water table shown in Figure 1(b). In addition to the cyclic and lateral loading studies, comprehensive programmes of dynamic and monotonic axial experiments were undertaken on 27 piles. Most were equipped with diametrically opposed strings of Fibre Bragg Grating (FBG) fibre-optical axial strain gauges, configured and processed as recommended by Doherty et al. (2015) and Burd et al. (2020). The influences of groundwater conditions, pile material, length (L), diameter (D) and wall thickness (t_w) on soil resistance to driving (SRD), set-up, loading sense (i.e. tension or compression) and long-term axial load-displacement behaviour were examined systematically over four years.

St NICHOLAS-AT-WADE SITE

The test site comprises a former quarry, located ≈2km inland and 15km west of Margate, Kent at UK Grid: TR 25419 66879. Buckley et al. (2018a) and Vinck et al. (2022) describe the Margate and Seaford white chalks encountered and provide full details of the chalk's geotechnical profiles and properties as measured through intensive in-situ and laboratory testing. They also note that tectonism, periglacial activity, weathering and geomorphology control the chalk's structure. Most weathered material has been removed leaving CIRIA grade B2 (Lord et al., 2002) structured, very weak-to-weak, low-to-medium density white structured chalk with closed-to-slightly open stained joints and beds of 250 mm average thickness, along with mainly vertically oriented micro-fissures spaced at 10 to 25mm apart.

The water table lies at ≈5.5 to 6m depth, ≈0.9m above Ordnance Datum (AOD); suctions measured at 3m depth with in-situ 'ICON' tensiometers fluctuated around 30kPa. Vinck et al (2022) report on the piezocone (CPTu) and Seismic CPT (SCPT) soundings undertaken close to each pile, nine of which are shown in conjunction with the pile tests reported later in this paper. Vinck et al (2022) also report on cone-pressuremeter testing, P-S logging, cross-hole and down-hole seismic testing and provide profiles of index, oedometer, simple-shear, unconfined compression and Brazilian tension tests. Multiple locally-instrumented (drained and undrained) triaxial tests were conducted on block samples and cores from Geobore-S wireline rotary boreholes. Vinck et al.,'s (2022) analysis of the data included detailed assessments of sample size effects and small-strain stiffness anisotropy. Liu et al. (2023) report further on the chalk's behaviour under cell pressures up to 13 MPa, as develop beneath the pile tips during driving.

Accepted manuscript doi:
10.1680/jgeot.22.00041

An additional highly relevant topic is how effective normal stress level, interface material, ageing, corrosion, and testing procedure affect the interface shearing resistance and shaft radial stress conditions developed around steel piles driven in chalk. Laboratory research by Vinck (2021) found that corrosion affects ultimate δ'_{ult} mildly, giving angles that exceed de-structured chalk's critical state $\phi'_{cs} \approx 31^{o}$ for all cases except (in the short-term) stainless steel. However, corrosion is shown later to affect axial capacity markedly through, it is argued, radial effective stress growth around corroding steel piles in a process comparable to that noted around steel bars in corroding reinforced concrete (Su et al., 2015). The reactions draw in additional air, water and salt molecules to generate lower density products that expand out, while being constrained radially by very stiff chalk. Noting that air can flow through any open fissures available above the water table, and the need to capture offshore conditions, Vinck (2021) examined how air and salinity affect surface corrosion mass loss rates of prismatic samples (termed coupons) cut from typically rough pile shaft in contact with chalk. The reaction rates developed over periods up to 67 days, expressed in μm steel loss per year, were:

- Ten times slower in isolated tests than when exposed to air.
- Three or more times faster with saline than fresh groundwater.
- Comparable between various oxidisable construction steels.
- Ninety times slower with stainless steel and absent with concrete.

Other laboratory testing by Doughty et al (2018) showed that the stiffness and shearing resistances of chalk that is de-structured to putty increase over time through both consolidation and carbonate re-bonding.

TEST PILES

Tables 1 to 3 summarise the considered test piles' sizes, tip conditions and materials. Fibre Bragg Grating (FBG) strain gauges, with the 0.15 to 0.6m spacings detailed in Table 4, were installed and monitored following the protocols set out by Doherty et al (2015) and gave high-resolution measurements over the piles' 3.05 to 18m embedded lengths. Applying temperature-corrections and Savitzky-Golay filtering to reduce scatter led to well-defined average axial force profiles from which local shaft resistances were generated. The latter accounted for pile plus chalk plug weights and upthrust due to any positive base water pressures. All but one of the monotonic tests considered tension loading conditions. All piles that were subsequently extracted showed fully retained internal cores with clean tension fractures at their bases. The average long term internal skin friction required to lift the internal cores was ≈2 kPa for the longer LD piles and ≈8 kPa for the largest (1.8m OD) ALPACA Plus pile. The distributions of internal shaft friction developed during the single compression test are not known and are implicitly included in the overall base and shaft resistances indicated by the FBG strain gauges. Tests reported by Vinck (2021) on other open instrumented steel piles driven in chalk, including one whose internal chalk core had been removed prior to testing, indicate that internal shaft resistance alone could not explain their higher compressive-than-tension axial shaft capacities.

Multiple Mitutoyo SJ-210 gauge measurements were made on the ALPACA piles that indicated pre-driving Centre-Line-Average R_{CLA} pile shaft roughness means of 15.4, 10.1 and 14.2μm for the oxidisable-steel LD, SD and ALPACA Plus piles respectively, while the stainless steel and concrete shafts gave 6.0 and 3.8μm. Noting the chalk's ≈3μm D_{50} grain size, all pile shafts provided fully rough interfaces; see Lings and Dietz (2005).

Large Diameter (LD) ALPACA series

The open-ended, oxidisable X80 steel, FBG instrumented, tubular LD piles had 508mm outside diameters (D) and 20.6mm wall thicknesses (t_w), giving relatively low $D/t_w \approx 24.7$. Most were driven in November 2017 to tip depths of 3.05m (≈3m above the water table with $L_p/D = 6$) or 10.16m (≈4.2m below the water table with $L_p/D = 20$).

Accepted manuscript doi:
10.1680/jgeot.22.00041

Smaller Diameter (SD) ALPACA series

The SD series included twelve 139mm diameter steel tubular piles (two with FBG strings) fabricated from various steels, driven to tip depths just above the water table. Ten open piles were driven from ground level to $38 < L_p/D < 40$; their 8 to 10mm wall thicknesses gave $14 < D/t_w < 17.5$. Tip conditions were investigated by driving two otherwise identical closed-ended steel SD piles. A 200mm square pre-cast reinforced concrete pile, with D* = 226m and $L_p/D^* \approx 24$, based on equivalent base area, and a pair of 'crenulated' SM-J steel sheet piles were also driven, with $L_p/D^* \approx 18$ to 19 when D* is defined from perimeter length/π = 290mm.
Four further 12m long, 139mm OD open-steel, piles and one additional 200mm factory pre-cast concrete pile, were driven to 6.15m through pre-bored cased holes that isolated their shafts from the unsaturated chalk.

ALPACA Plus series

The ALPACA Plus piles had higher D/t_w ratios (41 to 72) and 508mm, 1220mm and 1800mm outside diameters. Axial testing in October 2021 concentrated on piles driven to L_p =18m, with $10 \leq L_p/D \leq 35$. Table 3 details how Beginning of Re-drive (BoR) dynamic data recorded over the first blows applied after operational driving pauses, and at two later dates.

ANALYSIS OF DRIVING BEHAVIOUR

The open-tubular LD and SD piles required 9-to-55 blows per quarter metre (bpqm) with the hammers detailed in Table 5 and had total driving times of 2 to 14 minutes. All open piles generated chalk cores that rose well above ground level, confirming relatively little radial displacement out into the chalk mass. Figure 2 shows how the volume extruded above ground compared to that of the embedded steel, V_{pag}/V_{steel}, fell systematically with L_p/D; open-pile cores rarely rise above ground level in sands and clays.

The 200mm square concrete piles required up to 308 bpqm over up to 81 minutes to reach target depth with the hammers deployed; the sheet piles required up to 100 bpqm and ≈20 minutes of driving. Table 5 summarises estimates for the average non-dimensional velocity $V = vD^*/c_h$ (with v = final penetration/driving time) adopting piezocone dissipation test $c_h = 7 \times 10^{-4}$ m^2/year (Vinck et al., 2022), and D =2R* for open piles, after Carter et al. (1980). Finnie and Randolph (1994) argue that penetration is fully undrained for V>30 and principally undrained beneath closed-ended piles if V ranges from 2 to 20. Table 5 indicates low degrees of drainage during driving beneath the larger open-piles and higher degrees for the concrete and sheet piles. Dissipation tests at SNW with 43.7mm diameter piezocones showed pore pressures sensed at the cone shoulders dissipating fully within 80s. Scaling up by $(D^*/D_{CPT})^2$ leads to t_{95} estimates for the pile tip areas ranging from ≈400s to ≈2 hours for the smallest to largest diameter piles. As listed in Table 5, substantial dissipation is likely to have occurred over the driving pauses identified in Table 3.

Pile Driving Analyzer (PDA) strain-gauges and accelerometers were mounted on all piles and recorded at 40kHz. Iterative wave matching analyses, which applied the shaft and base resistance models in IMPACT (Randolph, 2008), indicated how shaft shear stresses evolved locally as pile tips advanced. Buckley et al. (2020b) considered both FBG and PDA measurements and describe how modelling parameters were selected and shaft resistances taken as applying over only the outside shaft areas. The FBG measurements agreed well with high-frequency conventional PDA measurements and the end-of-driving (EoD) datasets provided key information on the piles' initial axial resistance profiles. Buckley et al. (2020b), Cathie et al. (2022) and Wen et al (2023) show that rigorously conducted stress wave matches provide the best available proxy means of measuring instantaneous EoD resistances, which cannot be measured statically in cases where set-up progresses rapidly. These authors show that, if conducted and interpreted carefully, stress-wave analyses of instrumented dynamic re-strike tests provide shaft capacity estimates that are compatible with trends inferred from static testing. However, dynamic testing offers the only practical means of monitoring rapid early-age set-up, such as occurs in chalks.

Accepted manuscript doi:
10.1680/jgeot.22.00041

Tables 1 to 3 summarise the interpreted overall End of initial Driving (EoD) shaft and base resistances, while Figure 3 (a-e) illustrates the various series' EoD shaft friction profiles. Piles SD20 (open-steel), SD5 (closed-steel) and SD19 (concrete) represent the SD cases. The long and short 508mm piles are typified by LD5 and LD13; traces are also shown for the TP1 and TP3 ALPACA Plus piles. The open piles' average, compressive, τ_{avg}^{EoD} range from 19.8 to 32.2 kPa (including six 'SD' piles from Buckley et al. (2018a)) giving means and CoV of 24.8kPa and 0.14 respectively. Also shown are representative q_t traces from nearby CPTs and Chalk ICP-18 SRD predictions from Equations 1 and 2, which capture the local shear resistances' sharp reductions with increasing h/R*.

$$\tau_{rzi} = \sigma'_{ri} \tan\delta'_{ult} \qquad (1)$$

$$\sigma'_{ri} = 0.031 q_t \left(\frac{h}{R^*}\right)^{-0.481\left(\frac{D}{t_w}\right)^{0.145}} \quad (h/R^* \geq 6) \qquad (2)$$

Comparison of the total EoD shaft load between the predictions Q_s integrated from the above expressions, taking $\delta'_{ult} = 32^\circ$ and the signal-matching outcomes indicated a mean calculated-to-measured (Q_c/Q_m) ratio of 1.00 (with CoV = 0.38) for the open-ended piles listed in Tables 1-3 with reliable τ_{avg}^{EoD} values. Open piles with the lowest L_p/D (=6) values developed the highest EoD resistances, reflecting their lower h/R* values and consequently lesser local τ_{rzi} reductions. Closed-ended steel SD5 showed the lowest (reliable) τ_{avg}^{EoD} value, which fell well below the ICP-18 predictions, reflecting the larger strains and greater de-structuration that develop beneath closed pile tips. Baligh et al. (1987) showed strains reduce systematically with D/t_w during undrained penetration and are typically an order of magnitude smaller under open-tubular than closed-ended piles. The sheet and concrete piles' τ_{avg}^{EoD} (37.1 and 83.3 kPa respectively) matched ICP-18 estimates more closely, although their slow driving may have permitted more drainage; lower SRDs might have applied under undrained conditions.

Figure 4 presents the signal-matched EoD q_b values, evaluated over closed piles' full areas and open piles' annuli, normalised by q_t (averaged within 1.5D of the pile tip) and plotted against D/t_w (taking 2 for closed piles). The EoD q_b/q_t ratios decline with D/t_w as expected by Baligh et al. (1987), up to D/t_w ratios of at least 25. Equation (3) leads to a better and more conservative fit to the data than the Chalk ICP-18's tentatively suggested $q_b/q_t \approx 0.6$.

$$\frac{q_b}{q_t} = \left(D / t_w\right)^{-0.175} \qquad (3)$$

Pile set-ups were gauged by monotonic and (for ALPACA Plus) dynamic BoR tests. Noting that the 5.2 day re-strike on R2 may have set-back its subsequent ageing, the 421-day BoR provides a lower bound to the long-term resistance of an equivalent 'virgin' pile, although Vinck (2021) noted that the impact of early re-strikes diminish over time. Figure 5 plots against age the average re-strike set-up factors derived from BoR tests conducted on piles whose capacities were primarily developed below the water table, divided by the EoD value from the last blow before any pause commenced, along with t_{95} times estimated by scaling up the piezocone dissipation test t_{95} times by $(D^*/D_{CPT})^2$ as explained earlier. The normalised depths L_p/D, to which tips had advanced before each 'test' are also indicated. Table 5 identifies the early-age time ranges over which re-consolidation contributed to set-up. Set-up varies with L_p/D, as noted in full-scale offshore Wikinger pile tests by Buckley et al. (2020). The average set-up trend from eight Wikinger piles covering $0.26 \leq L_p/D \leq 14.9$ with a mean ≈6.8 is shown plotting close to the $L_p/D = 10$ SNW trend-curve in Figure 5. Tentative L_p/D contours are plotted whose interpretation combined: (i) BoR data, (ii) trends from the monotonic tension tests described below (accounting for the tension-to-compression shaft capacity ratio) and (iii) BoR tests on multiple 0.61m diameter open-steel piles driven in 2021 at Tilbury ≈70km east in the (same) Margate and Seaford formations (Wang, 2021).

Accepted manuscript doi:
10.1680/jgeot.22.00041

Further insight into early age set-up is given in Figure 6, where Pile R2's signal-matched τ_{rzi} EoD and three BoR τ_{rz} profiles are compared, covering its first re-strike (with L_p =7.2m) and two later restrikes performed after finally driving to 18m.

MONOTONIC TESTING

The tension tests all reacted against steel, concrete or timber surface pads, except for TP1, which required reaction piles. Reaction piles and kentledge were also employed for the single compression test. Figure 7 shows main components of the testing systems deployed. Displacements were recorded by at least three transducers, referenced to distant datums and placed at equal angles about the pile axis. Potentiometer devices were used for the LD series tests while linear variable differential transformers (LVDT) were employed for SD tests. Awnings reduced the impact of sun and wind variations. Hydraulic jacks applied steady loading between maintained load stages, whose durations gradually extended to an hour once creeping became significant. Load cell calibrations were checked when required and failure was defined by semi-logarithmic creep movement rates (k_s) remaining >2mm/log (t) one hour after applying the last load step. Most tests involved 8 to 10 load stages and ended within a day.

The piles showed apparently near linear load-displacement behaviour up to relatively (<6 kPa) low threshold τ_{avg} values. Analysis of the global initial linear response stages of the ALPACA tests made through Randolph & Wroth's (1978) approach, re-derived for tension, led to the results listed in Table 6. Overall, the global operational shear moduli, covering all zones, found over the limited linear range amounted be around 1/4 of corresponding seismic CPT G_{vh} values. Matthews et al. (2000) noted similarly marked discrepancies applying to shallow foundation loading in chalk, which they ascribed to natural discontinuities.

The piles' average shaft shear stresses τ_{rz} values at failure varied widely, from below 11 to over 200 kPa, depending on multiple factors. The analysis below considers separately piles installed entirely (i) above or (ii) below the water table and (iii) those that spanned both conditions.

Above the water table

Load tests are summarised as curves of average τ_{rz} against non-dimensional pile head displacement w/D, or w/D* for concrete and sheet piles, whose shear resistances were evaluated over their true perimeter areas. The open-ended, steel SD piles' first-time, tension loading curves are presented in Figure 8 along with tests by Buckley et al. (2018a) on identical piles. Average τ_{rzf} failure values varied from 30.2 to 142.3kPa, with the w/D ratios at which the maximum load was obtained increasing from ≈0.02 to 0.07 as the piles' aged.

Inert stainless-steel open pile

The stainless-steel SD18 pile developed the lowest tension τ_{rzf}, which was only 20% greater than its (compressive) EoD τ_{rzi}. If we treat, after Vinck (2021), compression shaft capacities as double those in tension, then the like-for-like set up ratio $\Lambda(t)$ is $2[\tau_{rzf}$ (tension)$/\tau_{rzi}$ (compression)$] \approx 2.4$ after 125 days.

Oxidisable steel open-piles

The oxidisable S355, L80/N80 and Drill casing open SD piles developed far higher $\Lambda(t)$ factors. Assuming again a compression/tension ratio =2, piles SD12 and DP6-T1 showed, after 318 and 246 days respectively, the highest ≈154.1 ± 15.5kPa resistances and maximum $\Lambda(t) = 8.15$. Interface shear tests against oxidisable X80 and S355 steels showed chalk δ'_{ult} angles growing modestly from ≈32^o to ≈34.5^o after long-term ageing with access to air and water (Vinck, 2021). So other processes, which do not act around stainless-steel piles, such as radial effective stresses building as corrosion products expand out radially into the very stiff chalk mass, are required to explain the oxidisable piles' long-term set-up above the water table.

Hammer size also affected the piles' end-of-driving resistances and long-term capacities. Buckley et al.'s (2018a) piles, driven with an 4ton Junttan SHK100-4 hammer that was 2.5 times heavier than that adopted for the ALPACA SD installations (see Table 4), gave particularly high long-term resistances and Λ values. Carroll et al. (2020) noted similar trends with piles driven in sand. Each

Accepted manuscript doi:
10.1680/jgeot.22.00041

hammer blow applies an extreme load cycle; it is plausible that less de-structuration occurs beneath pile tips and around shafts when larger hammers deliver significantly lower blow counts.

Figure 9 explores local shaft capacity trends by comparing the 318 days age tension τ_{rzf} profile deduced SD12's FBG strain gauges with its dynamic (compression) EoD profile from Figure 3(a). Set-up is evident over the whole shaft and most intensive over the mid-section. Also shown is a Chalk ICP-18 prediction evaluated employing the 'long-term' expressions given by Jardine et al (2018) and Buckley et al (2000) with $\delta'_{ult} = 32^o$. While the latter offers a similar shape to the field data, integration indicates non-conservative overall calculated-to-measured capacity ratios, $Q_c/Q_m \approx 1.74$ and ≈ 1.14 for SD12 and DP6-T1 respectively. As set out further below, these and other results identified a clear need to revise the Chalk ICP-18 procedures.

Closed-ended steel and concrete piles

Sampling and laboratory testing, undertaken after the pile experiments, identified the annular zone of chalk that had consolidated to far lower water contents after being reduced to putty by driving. The zone extended out to $\approx D/2$ (or $D^*/2$ for square piles) and to far smaller distances $\approx t_w$ around open piles.

Figure 10 presents the long-term tension load-displacement plots for three closed-ended piles. The 73.4kPa τ_{rzf} achieved by the closed-steel SD5 indicates an early-age $\Lambda = 7.45$ after pore-pressure and local stress equalisation (assuming again a compression/tension ratio =2), far above the average short term $\Lambda = 2.7$ shown by the lower-displacement open piles. Long-term ageing added a further 53kPa of tension shaft resistance to the twin SD7 pile over 329 days, giving a remarkable long-term 'compression' $\Lambda(t) = 14.4$.

The solid and inert (factory) pre-cast reinforced concrete pile, whose driving permitted greater pore pressure dissipation during driving, also showed a relatively high (125kPa) long-term tension resistance, reflecting the combined effects of its high driving resistance, post-EoD residual excess pore-pressure dissipation and potentially in-situ carbonate bonding; see Neugebauer (1975). However, assuming the compression shaft capacity was double that in tension (as with steel piles) indicates a lower long-term $\Lambda(t) \approx 3$ than was developed by the more rapidly driven, and actively corroding, closed steel pile. The closed-end piles failed with $0.03 < w/D < 0.07$ and their relatively high shaft capacities gave an average $Q_c/Q_m \approx 1.0$ when compared to Chalk ICP-18 predictions.

The sheet pile tests also showed remarkable set-up. SD10's tension resistance rose well above its EoD compression capacity when, after three days, it could not be failed with the equipment deployed. Corrosion led to a 35% stiffer load-displacement curve after 317 days for the twin SD9 sheet pile and a remarkable average $\tau_{rzf} > 205$ kPa applying after a displacement ratio $w/D = 0.055$.

Short LD piles

Figure 11 presents the short 508mm OD X80 steel piles' curves after driving to 3.05m penetrations. Their τ_{rzf} profiles, deduced from FBG gauges, are given in Figure 12, with EoD wave matches from Figure 3(c) and long-term Chalk ICP-18 predictions. The piles failed with $w/D < 0.035$ and average (tension) τ_{rzf} around 3.9 times the compressive τ_{rzi} values, indicating long-term 'compression' $\Lambda(t)$ ratios ≈ 7.9 slightly below the SD piles' maxima and reflecting similar long-term processes above the water table, with set-up being greatest over the mid and lower shaft sections. Long-term ICP-18 calculations capture the maximum observed local resistances (up to 270 kPa), but again over-estimate the overall tension capacities, giving $Q_c/Q_m \approx 1.60$.

Piles driven entirely below the water table

The ALPACA programme included five piles driven through holes pre-bored and cased to avoid contact with unsaturated chalk. As shown in Figure 13(a), the slowly-driven, closed-ended, solid concrete SD17 ($L/D^* \approx 47$) developed higher long-term resistance below the water table than the equivalent concrete pile (SD19) above the water table. While tensile straining in SD17's 6.5m of free shaft length led to larger pile head movements, this inert pile's development of a 'compression equivalent' $\Lambda > 3.3$ was not affected by being submerged.

Accepted manuscript doi:
10.1680/jgeot.22.00041

In contrast, the far higher L/D (≈90) and consequent flexibility of the 139mm OD steel tubes led to these piles 'whipping' during driving which, as noted by Lord et al. (2002) can halve capacity in low-to-medium density chalk. The piles' 6.5m unrestrained free lengths allowed them to deflect easily during assembly and testing, potentially further damaging their axial capacity. Figure 13(b) presents their tension load-displacement curves after 126 to 129 days of ageing, all failing at average low τ_{rzf} (10.7 to 18.7 kPa) and w/D < 0.03. Stainless-steel SD13 showed the lowest resistance. Assuming a compression-to-tension ratio of 2 indicates $\Lambda = 0.9$, well below the 2.4 applying (at a similar age) to the shorter and less flexible stainless-steel SD18 driven above the water table. The oxidisable high L/D piles showed greater capacities below the water table, indicating that corrosion also contributed (albeit modestly and slowly) to their set-up. Highly flexible piles driven with long unsupported sections clearly develop abnormally low capacities.

Piles with shafts above and below the water table

Long LD piles

Tension tests on open 508mm LD piles driven to 10.15m ($L_p/D = 20$) are presented in Figure 14, all failing with w/D <0.02. Average τ_{rzf} grew from 21.2 kPa (after 66 days) to 39.1 kPa at t > 200days, while the 'equivalent compression' long-term $\Lambda(t)$ values grew from ≈1.8 to ≈3.3 over the same age interval. Figure 5 collates their trends with those from other piles whose shaft capacities developed mostly below the water table. The compression test pile, LD7, illustrated in Figure 15, indicated Λ = 3.45 at 260 days, although the assessment depends on how loads are extrapolated over the lowest (0.65m) shaft length. Figure 15 also shows the average shear stresses evaluated for LD5, LD6 and LD7 down to the deepest strain gauge' the latter indicate tension τ_{rzf} values than Figure 14 because the final 0.65m contributes so heavily to capacity.

Much of the compression pile's greater resistance developed over its 0.005 < w/D < 0.075 range, where tangent stiffness slowly reduced towards zero at failure. This is interpreted as reflecting outward Poisson pile straining gradually raising shaft σ'_r and hence τ_{rzf} stresses as growing shaft and base loads compress the shaft and expand it radially. The compression-to-tension shaft capacity ratio from LD5 and LD6 is displayed in Figure 16 together with Vinck's (2021) assessment from similarly paired tests undertaken near Dieppe (France) and Hamburg (Germany) with comparable piles and chalks. An average ratio of at least 2 is indicated which, as discussed later, was confirmed by long-term ALPACA Plus tests.

The base capacity (1251.3 kN) mobilised at w/D = 0.075 was found by projecting loads to the tip depth. It exceeds the driving and short-term re-drive tip loads detailed in Tables 1 to 3, indicating significant set-up and a resistance q_b = 6.2 MPa over the entire base area ≈0.4q_t. Significant loads may have been transferred into the lowest section of the pile shaft through local internal shaft friction, as argued for sands by Jardine et al. (2005). Any internal shaft friction that develops above the lowest strain gauge level is effectively counted as combined with the external shaft resistance. Vinck (2021) provide further guidance based on long-term tests at other sites.

Local τ_{rzf} profiles are plotted in Figure 17 for LD5, 6 and 7. Also shown are the typical EoD profile from Figure 3(c) and long-term Chalk ICP-18 predictions. The compression test shows notably higher shaft resistance over its top half, where corrosion was most active, and the pile axial loads (and hence Poisson strains) were greatest. Nevertheless, the long-term Chalk ICP-18 predictions exceed the compression shaft capacity by 60% and those of the tension tests by a larger margin.

ALPACA Plus piles driven to 18m depth

The 18m long TP1 and TP3 piles' tension tests, conducted 373 and 380 days after driving, reached failure with w/D ≈0.02, as shown in Figure 14. Their set-up trends are identified in Figure 5, while Figure 18 presents their EoD and monotonic test τ_{rzf} profiles.

Sharp reductions in local resistance with h/R led to the 1800mm diameter ($L_p/D = 10$) TP1 pile's average tension τ_{rzf} (57.0 kPa) being more than double that (24.9 kPa) of the 508mm diameter TP3, whose $L_p/D = 35.4$. Figure 18 shows the local profiles that led to a 'compression equivalent' $\Lambda(t) = 4.31$ for TP1, which exceeds the ≈3.4 reached by LD piles (with $L_p/D = 20$), while TP3, the most slender pile, gave $\Lambda(t) = 1.85$. As shown in Figure 5, set-up declines with L_p/D. Chalk ICP-18 calculations for the TP1 and TP3 tension tests give Q_c/Q_m as 2.6 and 4.0 respectively.

The 421-day re-strike on the 18m long, 1220mm OD, R2 pile indicated average τ_{rzf} = 117.4 kPa in compression, 2.1 times TP1's tension resistance (57.0 kPa), supporting the Figure 16 compression-to-tension capacity trend. A still higher ratio may be inferred if allowance is made for R2's higher, and less advantageous, L_p/D.

Overall trends

The ALPACA and ALPACA Plus axial tests identified ten clear trends:

1. Open-ended and sheet steel piles develop notably lower driving resistances than closed steel and concrete piles.
2. Piles driven at the same site show average long-term τ_{rzf} values ranging from <11 kPa to >200 kPa.
3. Closed-ended piles displace and de-structure a more extensive region of chalk than open piles. This feature may explain their far higher driving and long-term shaft resistances, as implied (for example) by cylindrical cavity expansion analyses of pile installation effects, see Randolph et al., (1979) or Carter et al., (1980).
4. Highly flexible piles that 'whip' during driving develop anomalously low long-term shaft capacities.
5. Short and long-term shaft resistances fall steeply with h/R* or h/R in all cases.
6. Marked set-up commences immediately after driving as pore pressures dissipate and total stresses evolve towards equilibrium values under the highly kinematically constrained conditions applying near the pile shafts.
7. Further long-term set-up takes place above and below the water table at gradually slowing rates.
8. Corrosion reactions lead to set-up being notably faster (i) around oxidisable steel piles driven above the water table and (ii) with saline rather than fresh groundwater.
9. Compression shaft resistances appear to be at least twice as high as those available in tension.
10. Chalk ICP-18 predicts driving SRD resistances with no overall bias and relatively low scatter, but over-predicts long-term capacity in most cases, indicating a need for careful re-calibration.

Accepted manuscript doi:
10.1680/jgeot.22.00041

RECALIBRATION OF LONG-TERM ICP CAPACITY METHOD

The ALPACA and ALPACA Plus axial tests confirmed key general features of ICP-18's long-term shaft capacity formulation. However, they also proved the approach required significant recalibration to address the ten points itemised above. The first step was to expand the Coulomb criterion applied to characterise local shaft failure to recognise the impact of loading sense (compression or tension) on shaft capacity as shown in Equation 4.

$$\text{Local } \tau_{rzf} = f_L[\sigma'_{rc} + \Delta\sigma'_{rd}] \tan \delta' \qquad (4)$$

For simplicity, loading factors f_L of 2/3 and 4/3 are taken for tension and compression that ensure a shaft capacity ratio of 2. These factors could be refined as further field or theoretical evidence emerges.

Updating is also required for the $\Delta\sigma'_{rd}$ interface dilation term. As highlighted in Table 6, elastic analysis of the pile tests shows the maximum elastic shear stiffness G_{vh} under pile loading is only 1/4 of that expected from seismic CPT testing. Adopting Lings and Dietz's (2005) finding that shearing against fully rough interfaces induces a normal (dilative) displacement Δr in granular media comparable to their D_{50} grain size under the stress levels applying around pile shafts in chalk, leads to Equation 5. Iterative analysis indicates that Δr may be taken as ≈5μm and ≈3μm above and below the water table respectively.

$$\Delta\sigma'_{rd} = 4G_{ope}\Delta r/D \qquad (5)$$

Applying Vinck's (2021) $\delta' = 32^o$ and Equations (4) and (5) to the τ_{rzf} - depth profiles presented in Figures 9, 12, 17 and 18 leads to the pre-loading σ'_{rc}/q_t versus h/R trends in Figure 19 (a) and (b) for conditions above and below the water table respectively. The fitted power law relationships, given as Equations 6 and 7, are subject to h/R minima, below which σ'_{rc}/q_t is constant. They capture markedly steeper σ'_{rc}/q_t decays with pile tip depth than Chalk ICP-18. They also employ h/R without any effective area term being required to avoid skewing with respect to D/t_w over the 15.4 to 80.8 range considered. Alternative correlations with h/R* lead to marginally less satisfactory outcomes.

$$\text{Above water table: } \sigma'_{rc}/q_t = f_{tip}\times 0.078\times(h/R)^{-0.85} \ (h/R \geq 4.0) \qquad (6)$$

$$\text{Below water table: } \sigma'_{rc}/q_t = f_{tip}\times 0.025\times(h/R)^{-0.80} \ (h/R \geq 0.5) \qquad (7)$$

The pile-tip factor f_{tip} is 1 for the open piles considered and 3 for closed-ended piles. Intermediate factors may apply over the unexplored $2 \leq D/t_w \leq 15.4$ range. Any 'internal' shaft resistance developed by open piles under compression loading is assumed to be built into these shaft and end bearing expressions; both sides of sheet piles are considered.

Integrating Equations 4 to 7 over the pile shafts provides capacity predictions for sixteen ALPACA, ALPACA Plus and Innovate UK (Buckley et al., 2018a) axial pile tests conducted at ages ≥120 days at the SNW site. Two deliberately 'non-standard' stainless-steel piles (SD13 and 18) were excluded, so were the very high L_p/D open-ended steel SD piles driven through cased holes that had experienced whipping during installation. Table 7 summarizes the mean Q_c/Q_m found with the recalibrated long-term approach for this dataset, showing unbiased means and relatively low CoVs for piles driven either entirely above or below the water table as well as those that span both conditions. In comparison, the CIRIA (Lord et al., 2002) method is systematically over-conservative and Chalk ICP-18 non-conservative, largely because of the latter's assumption of equal tension and compression shaft capacities and less steep 'friction-fatigue' relationship. Set-up factors Λ, which vary strongly with L_p/D, may be assessed by dividing the calculated long-term capacities by the SRD values, which are generally well-predicted by Chalk ICP-18.

The individual pile test points plotted in scatter diagrams in Figure 20 confirm that the new method gives no significant bias with diameter D, length L_p, L_p/D, wall thickness ratio, D/t_w or time over the ≥ 120 days age range.

Accepted manuscript doi:
10.1680/jgeot.22.00041

Research remains active to assess how well the ALPACA-SNW approach predicts pile tests at other chalk sites, drawing on the case studies collated and reviewed by Vinck (2021) and other data. Further checking at other locations and in denser chalk strata is recommended.

SUMMARY AND CONCLUSIONS

The ALPACA and ALPACA Plus JIP programmes addressed the uncertain behaviour of piles driven in low-to-medium density chalks through comprehensive dynamic, cyclic, monotonic, axial and lateral testing of piles covering a wide range of scales, materials, groundwater conditions, ages and loading modes, generating a unique high-quality experimental database against which design approaches may be assessed and developed. Buckley et al. (2023) report the cyclic axial pile loading experiments and show how their responses may be predicted from laboratory element tests and ALPACA AWG (2022) summarised the lateral loading study.

The main outcomes regarding monotonic axial loading are:

1. Evidence of, and explanations for, a remarkably wide range of axial shaft resistances with: (i) pile end-conditions and material, (ii) L_p/D ratio and flexibility, (iii) relative water table depth, (iv) age after driving and (v) whether loading is compressive or tensile.
2. Parallel information on load-displacement behaviour in tension and compression.
3. Demonstration that driving resistances are generally well predicted by Chalk ICP-18, while long-term capacity prediction methods are over-predicted by this approach. The CIRIA approach is shown to be generally over-conservative.
4. A new ALPACA-SNW approach is proposed which fits far more satisfactorily the widely ranging axial capacities measured at SNW on piles driven above or below the water table, when tested after at least 120 days after driving.
5. Independent checking is underway to explore how well the approach performs in predicting research tests conducted at other sites in France, Germany and the UK; further high-quality testing at other sites is strongly recommended.

Acknowledgements

The Authors gratefully acknowledge support from Engineering and Physical Science Research Council (EPSRC) grant EP/P033091/1, Royal Society Newton Advanced Fellowship NA160438 and Supergen ORE Hub 2018 (EPSRC EP/S000747/1). Byrne is supported by the Royal Academy of Engineering under the Research Chairs and Senior Research Fellowships scheme, while Vinck was supported by EPSRC Grant EP/L016826/1, DEME and Imperial College. The provision of additional financial and technical support by the following project partners is also acknowledged gratefully: Atkins, Cathies, Equinor, Fugro, GCG, LEMS, Ørsted, Parkwind, RWE, Siemens-Gamesa, Scottish Power Renewables and Vattenfall. The Authors also wish to acknowledge Socotec UK Ltd as their main contractor for the field-testing programme, Marmota Engineering AG as the fibre optic strain gauge specialists. Cambridge in situ for the pressuremeter tests and Lankelma UK and Fugro Geo-services for in-situ testing and rotary boreholes.

Accepted manuscript doi:
10.1680/jgeot.22.00041

List of notation

Roman alphabet

ALPACA Axial-Lateral Pile Analysis for Chalk Applying multi-scale field and laboratory testing
AOD Above Ordnance Datum
BoR Beginning-of-Restriking
CPT Cone penetration test
c_h Coefficient of horizontal consolidation
CoV Coefficient of variation
D Diameter of pile or penetrometer
*D** Equivalent pile diameter based on base area for cylindrical and square piles, and perimeter area for sheet piles
D_{50} Mean particle diameter
D/t_w Pile wall thickness ratio
EoD End-of-Driving
FBG Optical fibre Bragg grating strain gauge
FoS Factor of safety
f_s CPT sleeve friction
f_L Axial compression or tension loading factor
f_{tip} Open- or closed-end tip condition factor
G_{max} Maximum shear modulus
G_{vh} Shear modulus in the vertical plane
G_{ope} Operational shear stiffness
h Distance from the pile tip
k_s Increment of creep displacement per log cycle of time
L_p Pile embedded length
L_p/D Pile length ratio
PDA Pile Driving Analyzer
R Pile radius
q_t CPT cone resistance
Q_b Pile base capacity
Q_c/Q_m Calculated-to-measured pile capacity
R^* Open ended pile effective radius
R_{CLA} Centre-line-average surface roughness
SCPT Seismic cone penetration test
SNW Saint Nicholas-at-Wade (near Margate, Kent, SE England)
SRD Soil resistance to driving
S_u Undrained shear strength
t_w Pile wall thickness
t_{100} Full drainage elapsed time after end-of-driving
V Pile velocity

V Normalised velocity (= vD/c_h)

W Pile head displacement

Greek alphabet

δ', δ'_{ult} Ultimate interface friction angle

ϕ'_{cs} Critical state shear resistance angle

τ_{avg} Average shaft resistance

τ_{zf} Mobilised shaft resistance at failure

τ_{rzi} Shaft resistance at end-of-driving

σ'_r Radial effective stress

σ'_{rf} Radial effective stress at failure

$\Delta\sigma'_{rd}$ Change in radial effective stress due to interface dilation

Δr Radial dilation at pile interface

σ'_z Vertical effective stress

Λ Set-up factor

References

ALPACA AWG (2022). Monotonic and cyclic lateral loading of piles in low to medium density chalk. Report prepared by ALPACA Academic Work Group (AWG) for JIP Sponsors. Issued March 2022.

Baligh, M. M., Azzouz, A. S. & Chan, C. T. (1987). Disturbances due to ideal tube sampling. J Geotech Eng ASCE 113 (7), 739-757.

Barbosa, P. M., Geduhn, M., Jardine, R. J. & Schroeder, F. C. (2017). Large scale offshore static pile tests-practicality and benefits. Society for Underwater Technology: 8th International Conference on Offshore Site Investigation and Geotechnics, Smarter Solutions for Offshore Developments, London, UK, vol. 1, pp, 644-651.

Buckley R. M. (2018). The axial behaviour of displacement piles in chalk. PhD Thesis, Imperial College London, London, UK.

Buckley, R. M., Jardine, R. J., Kontoe, S., Parker, D. & Schroeder, F. C. (2018a) Ageing and cyclic behaviour of axially loaded piles driven in chalk. Géotechnique 68(2):146-161.

Buckley, R. M., Jardine, R. J., Kontoe, S. & Lehane, B. M. (2018b) Effective stress regime around a jacked steel pile during installation ageing and load testing in chalk. Canadian Geotechnical Journal 55(11):1577-1591.

Buckley, R. M., Jardine, R. J., Kontoe, S., Barbosa, P. & Schroeder, F. C. (2020a). Full-scale observations of dynamic and static axial responses of offshore piles driven in chalk and tills. Géotechnique, 70(8): 657-681.

Buckley, R. M., McAdam, R, A., Byrne, B. W., Doherty, J. P., Jardine, R. J., Kontoe, S. & Randolph, M. F. (2020b) Optimization of impact pile driving using optical Fiber Bragg-Grating measurements. Journal of Geotechnical and Geoenvironmental Engineering 146(9):04020082.

Buckley, R. M., Jardine, R. J., Kontoe, S., Liu, T., Byrne, B. W., McAdam, R. A., Schranz, F. & Vinck, K. (2023) Axial cyclic loading of piles in low to medium density chalk. Geotechnique. In press.

Burd, H. J., Beuckelaers, W. J. a. P., Byrne, B. W., Gavin, K. G., Houlsby, G. T., Igoe, D. J. P., Jardine, R. J., Martin, C. M., Mcadam, R. A., Wood, A. M., Potts, D. M., Gretlund, J. S., Taborda, D. M. G. & Zdravković, L. (2020) New data analysis methods for instrumented medium-scale monopile field tests. Géotechnique 70(11):961-969.

Carotenuto, P., Meyer, V., Strøm, P. J., Cabarkapa, Z., St. John, H. & Jardine, R. J. (2018). Installation and axial capacity of the Sheringham Shoal offshore wind farm monopiles – a case history. Engineering in Chalk: Proceedings of the Chalk 2018 Conference (Lawrence J. A, Preene M, Lawrence U. L. and Buckley R. M. (Eds)). ICE Publishing, London, UK, pp. 117-122.

Carroll, R., Carotenuto, P., Dano, C., Salama, I., Silva, M., Rimoy, S., Gavin, K. & Jardine, R. J. (2020) Field experiments at three sites to investigate the effects of age on steel piles driven in sand. Géotechnique 70(6):469-489.

Carter, J. P., Randolph, M. F. and Wroth, C. P. (1980) Some aspects of the performance of open-and closed-ended piles. *Numerical methods in offshore piling*. Pub ICE, London, pp 165-170.

Cathie D., Jardine, R. J, Silvano, R., Kontoe, S. and Schroeder. F (2022). Pile setup in sand – the "PAGE" joint industry project. Proc. 11th International Conference on Stress Wave Theory and Design and Testing Methods for Deep Foundations. Rotterdam. September 2022. https://community.kivi.nl/en/papers-stress-wave-conference.

Ciavaglia, F., Carey, J. & Diambra, A. (2017). Time-dependent uplift capacity of driven piles in low to medium density chalk. Géotechnique Lett. 7, No. 1, 90–96,

De Nicola, A. & Randolph M. F. (1993) Tensile and compressive shaft capacity of piles in sand. Journal of Geotechnical Engineering 119(12):1952-1973.

Doherty, P., Igoe, D., Murphy, G., Gavin, K. Preston, J., McAvoy, C., Byrne, B.W., Mcadams, R., Burd, H.J., Houlsby, G.T., Martins, M.C., Zdravkovic, L., Taborda, D.M.G., Potts, D.M., Jardine, R.J., Sideri, M., Schroeder, F. C., Muir Wood, A., Kallehave, D. and Skove Gretlund, J. (2015). Field validation of fibre Bragg grating sensors for measuring strain on driven steel piles. Géotechnique Letters 5, 74–79.

Doughty, L. J., Buckley, R. M. & Jardine, R. J. (2018). Investigating the effect of ageing on the behaviour of chalk putty. Engineering in Chalk: Proceedings of the Chalk 2018 Conference (Lawrence J. A, Preene M, Lawrence U. L. and Buckley R. M. (Eds)). ICE Publishing, London, UK, pp. 695-701.

Finnie I. M. S. & Randolph, M. F. (1994). Punch-through and liquefaction induced failure of shallow foundations on calcareous sediments. Proc. Int. Conf. Behaviour of Offshore Structures, Boston, Massachusetts: 217-230

Hobbs N. B. & Atkinson, M. S. (1993). Compression and tension tests on an open-ended tube pile in chalk. Ground Engineering, 26, No. 3: 31-34.

Jardine, R. J., Chow, F C, Overy, R. F & Standing, J. R (2005) ICP design methods for driven piles in sands and clays. Thomas Telford Ltd, London.

Jardine, R. J., Buckley, R. M., Kontoe, S., Barbosa, P. & Schroeder, F. C. (2018). Behaviour of piles driven in chalk. Engineering in Chalk: Proceedings of the Chalk 2018 Conference (Lawrence J. A, Preene M, Lawrence J. L., and Buckley R. M. (Eds)). ICE Publishing, London, UK, pp. 33-51.

Jardine, R. J., Kontoe, S., T., Liu, Vinck, K., Byrne, B. W., McAdam, R. A., Schranz, F., Andolfsson & Buckley, R. M. (2019). The ALPACA research project to improve design of piles driven in chalk. Improving the design of piles driven in chalk through the ALPACA research project. Proceedings of the 17th. European Conference on Soil Mechanics and Geotechnical Engineering, Reykjavik, Iceland.

Lings, M.L. & Dietz, M.S. (2005). The peak strength of sand-steel interfaces and the role of dilation. Soils and Foundations, Vol. 45, No. 6, pp 1-14.

Liu, T., Ferreira, P., Vinck, K., Coop, M. R., Jardine, R. J. and Kontoe, S. (2023). The behaviour of a low-to-medium density chalk under a wide range of pressure conditions. Soils & Foundations, 63(1), https://doi.org/10.1016/j.sandf.2022.101268.

Lord, J. A., Clayton, C. R. I. & Mortimore, R. N. (2002). Engineering in chalk, CIRIA, C574.

Matthews, M.C., Clayton, C.R.I. and Own, Y. (2000). The use of field geophysical techniques to determine geotechnical stiffness parameters. Proc. Inst. Civil Engnrs, Geotechnical Engineering, 143, (1), 31– 42.

Mortimore, R. N. (2013). The 11th Glossop Lecture: making sense of chalk: a total-rock approach to its engineering geology. Q. J. Engng Geol. Hydrogeol. 45, No. 3, 252–334.

Neugebauer, J. (1975). Some aspects of cementation in Chalk. Chapter 7 of 'Pelagic Sediments: On land and under the sea', pp 149-176. Editors, Kenneth J. Hsu and Hugh C. Jenkins. Pub. Blackwell Scinetific Publications. Oxford, UK.

Pedone, G., Kontoe, S., Zdravkovic, L., Jardine, R. J. (2020). Supergen ORE Flexible Funding Research Project ALPHA: Numerical analysis of laterally loaded piles driven in chalk. Final Report, Imperial College London, September 2020.

Pedone, G., Kontoe, S., Zdravković, L., Jardine R. J., Vinck K & Liu T. (2023). Numerical modelling of laterally loaded piles driven in low-to-medium density fractured chalk. (2023). Computers & Geotechnics, 156, 105252. https://doi.org/10.1016/j.compgeo.2023.105252.

Randolph, M. F. & Wroth, C. P. (1978) Analysis of deformation of vertically loaded piles. Journal of the geotechnical engineering division 104(12):1465-1488.

Randolph, M. F., Carter, J. P. and Wroth, C. P. (1979) Driven piles in clay. The effects of installation and subsequent consolidation. Geotechnique 29, No.4, pp 143-157.

Su, R. K. L. and Zhang, Y. (2015) A double-cylinder model incorporating confinement effects for the analysis of corrosion-caused cover cracking in reinforced concrete structures. Corrosion Science. 99: 205-218.

Vinck, K (2021) Advanced geotechnical characterisation to support driven pile design at chalk sites. PhD thesis, Department of Civil and Environmental Engineering, Imperial College London.

Vinck, K., Liu, T., Jardine, R. J., Kontoe, S., Ahmadi-Naghadeh, R., Buckley, R. M., Byrne, B. W., Lawrence, J., Mcadam, R. A. & Schranz, F. (2022) Advanced in-situ and laboratory characterisation of the ALPACA chalk research site. Géotechnique, published ahead of print, https://doi.org/10.1680/jgeot.21.00197.

Wang, Z. (2021) Static and dynamic re-analysis of large-scale pile tests in chalk. MSc dissertation, Department of Civil and Environmental Engineering, Imperial College London.

Wen, K., Kontoe, S., Jardine, R. J., Liu, T., Cathie, D., Silvano, R., Prearo C., Wei, S., Schroeder, F. C., and Po, S. (2023). Assessment of time effects on capacities of large-scale piles driven in dense sands. Ahead of Print in Canadian Geotechnical Journal, https://doi.org/10.1139/cgj-2022-0060.

Table 1 Summary for ALPACA LD open steel piles

Code	Steel grade	D (m)	t_w (mm)	L_p (m)	H_{plug} (m)**	EoD τ_{avg} (kPa)	EoD q_{ba}/q_t	Age† (Days)	Test τ_{avg} (kPa)	Comment‡
LD5	X80	0.508	20.6	10.16	0.96	21.1	0.47	219	36.7	
LD6	X80	0.508	20.6	10.16	0.88	28.0	0.52	211	39.1	
LD7	X80	0.508	20.6	10.16	1.02	20.4	0.58	260	59.7 (70.4)§	Compression
LD12	X80	0.508	20.6	3.05	1.07	31.3	0.40	221	112.0	
LD13	X80	0.508	20.6	3.05	0.99	19.8	0.42	294	89.2	
LD14	X80	0.508	20.6	10.16	0.90	24.8*	-	66	21.2	

*PDA data quality of LD14 assessed as poor following Buckley's (2018) approach so tabulated value represents the average EoD τ_{avg} for all LD piles.
**Chalk plug height above the original ground level.
†Age: at first 1st monotonic test.
‡Tests in tension unless otherwise noted.
§Average shaft resistance τ_{avg} = 59.7 kPa determined for top 9.5m embedded section directly from FBGs; τ_{avg} = 70.4kPa derived for full length, estimated from 9.5-10.16m section of tension tests (LD5 and LD6), assuming compression-to-tension ratio of 2.

Accepted manuscript doi:
10.1680/jgeot.22.00041

Table 2 Summary for ALPACA SD steel tubular piles

Code	Steel grade	D (m)	t_w (mm)	L_p (m)	H_{plug} (m)**	EoD τ_{avg} (kPa)	EoD q_{ba}/q_t	Age (Days)	Test τ_{avg} (kPa)	Comment‡
SD5	Drill casing	0.139	9.7	5.50	-	19.7	0.82	3	73.4	Closed
								276	81.3	Re-test
SD7	Drill casing	0.139	9.4	5.40	-	19.7*	-	330	142.3	Closed
								332	134.8	Re-test
SD8	Drill casing	0.139	9.6	5.44	0.56	26.0	0.73	2	57.5	Open
								308	55.4	Re-test
SD12	Drill casing	0.139	10.2	5.35	0.65	24.8*	-	318	69.3	Open
SD13	Stainless	0.139	8.0	5.42	≈ 0.46	25.8	0.67	126	10.7	Cased, open
SD14	Drill casing	0.139	9.8	5.31	≈ 1.30	22.5	0.59	127	13.1	Cased, open
SD15	S355	0.139	8.6	4.92	≈ 1.69	27.4	0.74	128	18.7	Cased, open
SD16	L80/N80	0.139	10.0	5.41	≈ 1.18	20.4	0.58	129	17.0	Cased, open
SD18	Stainless	0.139	8.0	5.49	0.26	24.8 *	-	125	30.2	Open
SD20	Drill casing	0.139	10.1	5.50	0.30	23.3	0.68	126	57.0	Open
SD21	S355	0.139	8.2	5.48	0.33	26.3	0.70	127	50.9	Open
SD22	L80/N80	0.139	9.6	5.48	0.0	24.5	0.72	128	51.0	Open

Continued Table 2 Summary for ALPACA SD closed-ended sheet and precast concrete piles

Code	Material	D_{equ}† (m)	t_w (mm)	L_p (m)	EoD τ_{avg} (kPa)	EoD q_b/q_t	Age (Days)	Test τ_{avg} (kPa)	Comment‡
SD10	Sheet/S355 steel	0.290	12.2	5.42	37.1	0.99	3	48.0	System limit, not failed
							170	146.2	Re-test, failed
SD9	Sheet/S355 steel	0.290	11.0	5.35	37.1*	-	317	204.7	System limit, Not failed
SD17	Precast concrete	0.255	-	4.93	83.3*	-	129	134.6	Not failed
							155	98.2	Re-test, failed
SD19	Precast concrete	0.255	-	5.40	83.3	0.89	156	126.1	Failed

*PDA data quality judged as poor following Buckley (2018) approach. Tabulated values represent: (1) either the average EoD τ_{avg} for all open-ended tubular pile cases, = 24.8kPa, or (2) EoD τ_{avg} of 'twin' pile(s) with similar geometry.
**Chalk plug height above the original ground level.

†Equivalent diameter D_{equ} = Perimeter/π.
‡Tests in tension unless otherwise noted.
Table 3 Summary for ALPACA Plus open steel series

Code	Material	D (m)	t_w (mm)	L_p (m)	H_{plug} (m)**	EoD τ_{avg} (kPa)	EoD q_{ba}/q_t	Age (days)	Type‡	Test or BoR τ_{avg} (kPa)	BoR q_{ba}/q_t
TP1	S355	1.8	25	7.94	-	22.8	0.40	0.09	Restrike	79.6	0.50
				18.0 (EoD)	1.41	26.2	0.61	373	AST	57.0	
TP2	S460	1.22	24.6	3.14	-	23.4	0.50	0.05	Restrike	63.0	0.60
				7.3 (EoD)	0.83	22.1	0.50	409	LS		
TP3	S355	0.508	12.5	7.90	-	24.8*	-	0.05	Restrike	59.3	0.50
				18.0 (EoD)	1.20	26.9	0.50	380	AST	24.9	
R1	S460	1.22	24.6	4.11	-	20.7	0.40	0.06	Restrike	66.0	0.60
				7.3 (EoD)	0.79	31.3	0.50	415	L1W/LS		
R2	S460	1.22	24.6	7.19	-	32.2	0.50	0.64	Restrike (BoR1)	64.1	0.60
				17.97 (EoD)	1.36	24.2	0.61	5.2	Restrike (BoR2)	76.2	0.73
								421	Restrike (BoR3)	117.4	0.82

*PDA data quality judged as poor following Buckley (2018) approach. Tabulated values represent: (1) either the average EoD τ_{avg} for all open-ended tubular pile cases, = 24.8kPa, or (2) EoD τ_{avg} of 'twin' pile(s) with similar geometry.
**Chalk plug height above the original ground level.
‡Test type: AST - Axial static tension; BoR - Beginning of restriking; LS - Lateral static; L1W - Lateral one-way cyclic, see McAdam et al. (2022).

Accepted manuscript doi:
10.1680/jgeot.22.00041

Table 4 Fibre Bragg Grating (FBG) sensor configuration

Series	Nr.†	Top (mbgl.)	Bottom (mbgl.)	Spacing	Temperature sensor depth (mbgl.)
SD12	12	0.12	5.08	≈0.28m to 1.23m bgl., then 0.55m	-
Short LD	12	0.15	2.85	0.15m to 0.75m bgl., then 0.3m	-
Long LD	12	0.5	9.5	0.5m to 2.5m bgl., then 1m	9.4 (only with LD14)
TP1, TP3	29 (+2)*	0.62	17.85	≈0.61m throughout	9.18, 17.8
TP2, R1	17 (+2)*	-0.15	7.15	≈0.33m to 2.15m bgl., then 0.5m	-0.15, 6.65 (only with TP2)

†Number of sensors in one FBG string; all piles instrumented with two diametrically opposite strings

*Value in bracket is number of temperature fibre optic temperature sensors.

Table 5 Ranges of normalised velocity V and upper bound full drainage elapsed times after end-of-driving

Series	Geometry/end condition	R^* (m)	Normalised V	Upper bound t_{95}(min)	Hydraulic hammer (ram mass)
SD	Open	0.035	0.52 - 1.50	3.4	Delmag (1.4 ton)
SD	Closed	0.070	0.36 - 1.20	13.4	
SD	Sheet	0.057	0.24	9.0	
SD	Concrete	0.113	0.10 - 0.16	35.5	
LD	Open	0.100	0.79 - 2.09	27.9	Juntann SHK-4 (4 ton) Juntann HHK-5A (5 ton)
ALPACA Plus (1.8m OD)	Open	0.211	2.74	123.4	BSP CG240 (16 ton)
ALPACA Plus (1.22m OD)	Open	0.171	1.64 - 2.48	81.8	BSP CX110 (9 ton)
ALPACA Plus (0.508m OD)	Open	0.079	0.50	17.2	

Accepted manuscript doi:
10.1680/jgeot.22.00041

Table 6 Operational shear moduli derived from linear elastic analyses of initial loading stages of monotonic pile tests

Pile	D (m)	L_p (m)	Initial pile stiffness (kN/mm)	G_{ope} (MPa)	G_{ope}/G_{max}	Note[†]
SD12	0.139	5.35	584.7	313.0	0.22	
LD5	0.508	10.16	2080.5	451.9	0.31	
LD6	0.508	10.16	1906.9	381.4	0.26	
LD7	0.508	10.16	1982.5	409.7	0.28	
LD12	0.508	3.05	1798.8	393.7	0.27	
LD13	0.508	3.05	1864.6	412.9	0.28	
TP1	1.8	18	3252.0	222.2	0.15	
TP3	0.508	18	1212.3	279.9	0.19	
TP2*	1.22	7.3	3554.4	364.2	0.25	Compression
R1*	1.22	7.3	3883.5	422.3	0.29	Compression

*TP1 loaded in tension, reacting against piles TP2 and R1.

[†]Tests in tension unless otherwise noted.

Table 7 Q_c/Q_m statistics for three axial capacity prediction methods, assessed against long-term monotonic measurements made in the ALPACA, ALPACA Plus and earlier Innovate UK (Buckley et al., 2018a) studies on 16 piles at SNW, excluding the stainless piles and the anomalous L/D = 90 SD pile outcomes

Method	Q_c/Q_m – whole shafts spanning water table depth			Q_c/Q_m – above water table			Q_c/Q_m – below water table		
	Mean	Standard deviation	CoV	Mean	Standard deviation	CoV	Mean	Standard deviation	CoV
CIRIA	0.33	0.16	0.49	0.42	0.29	0.69	0.37	0.16	0.43
ICP-18	2.06	0.91	0.44	1.97	0.95	0.48	2.96	0.87	0.29
New method	1.00	0.16	0.16	1.05	0.27	0.26	1.08	0.24	0.23

Accepted manuscript doi:
10.1680/jgeot.22.00041

Figure captions

Figure 1 Pile testing layout at SNW: (a) Plan (b) Section showing locations, diameters and levels relative to the water table for ALPACA LD, SD and ALPACA Plus piles.

Figure 2 Variation of the ratio between the above-ground chalk plug volume (V_{pag}) and embedded steel volume (V_{steel}) against L_p/D

Figure 3 Profiles CPT resistance and shaft friction from end-of-driving (EoD) PDA analyses against short-term Chalk ICP-18 predictions: (a) SD series: open-ended piles; (b) SD series: closed-ended piles; (c) LD series; (d) ALPACA Plus TP1; (e) ALPACA Plus TP3.

Figure 4 Normalised bearing pressure (q_b/q_t) against piles' D/t_w at end-of-driving (Note: q_b evaluated over the closed piles' full areas and the open piles' steel annuli; D/t_w taken as 2 for closed piles).

Figure 5 Variation with time of 'compressive' Λ set-up factors' for shaft friction from dynamic restrike and monotonic tension tests on (mainly submerged) ALPACA Plus and LD piles, showing L_p/D ratios and tentative contours. Average trend also shown from eight 'Wikinger' offshore piles with mean chalk $L_p/D = 6.8$, from Buckley et al. (2020a).

Figure 6 Short- and longer-term set-up shown by end-of-driving and beginning-of-restriking shaft resistance profiles of the ALPACA Plus pile R2 (see Table 3). CPT profile also shown.

Figure 7 Schematic arrangements for (a) tension and (b) compression pile tests.

Figure 8 Trends for average shaft resistance (τ_{avg}) against normalised pile head displacement (w/D) for open-ended SD piles embedded fully above water table

Figure 9 Comparison of shaft resistance profiles for SD12 determined from EoD PDA, short- and long-term Chalk ICP-18 predictions and FBG measurements at peak failure load. CPT profile also shown.

Figure 10 Trends for τ_{avg} against w/D (or w/D_{equ}) for closed-ended tubular steel and square concrete piles. ICP-18 predicts τ_{avg} = 163.0 and 145.1 kPa for SD7 and SD19.

Figure 11 Trends for τ_{avg} against w/D for LD12 and LD13 ($D/t_w \approx 24.7$; $L_p/D = 6$) embedded fully above water table. ICP-18 predicts τ_{avg} = 162.0 and 155.2 kPa for LD12 and LD13.

Figure 12 Short- and long-term shaft resistance profiles for LD12 and LD13 from EoD, long-term Chalk ICP-18 predictions and FBG measurements at peak failure loads. CPT profile also shown.

Figure 13 Trends for τ_{avg} against w/D (or w/D_{equ}) for (a) precast concrete piles and (b) cased SD13-SD16 steel piles embedded fully below water table. ICP-18 predicts τ_{avg} = 249.0 and 145.1 kPa respectively for SD17 and SD19, and on average 116.3 kPa for SD13-16.

Figure 14 Trends for tension τ_{avg} against w/D for the long LD piles and ALPACA Plus piles. ICP-18 predicts τ_{avg} = 141.5, 115.1, 99.5 and 144.5 kPa for LD5, LD6, TP3 and TP1 respectively.

Accepted manuscript doi:
10.1680/jgeot.22.00041

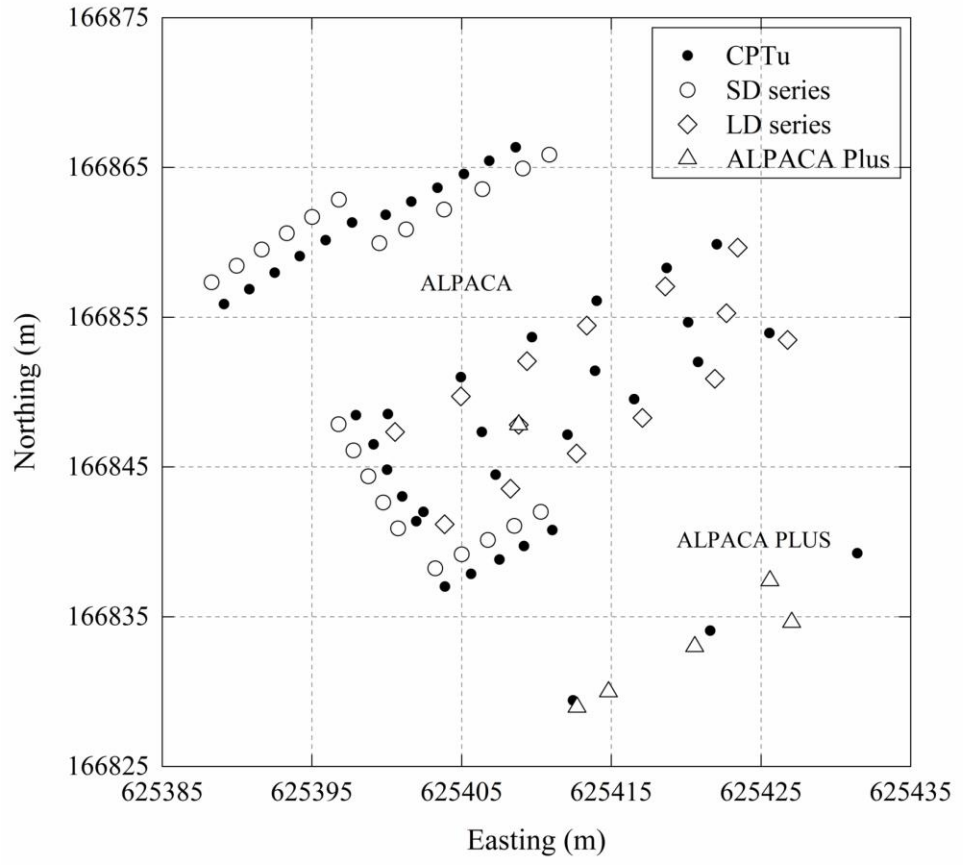

Figure 1(a)

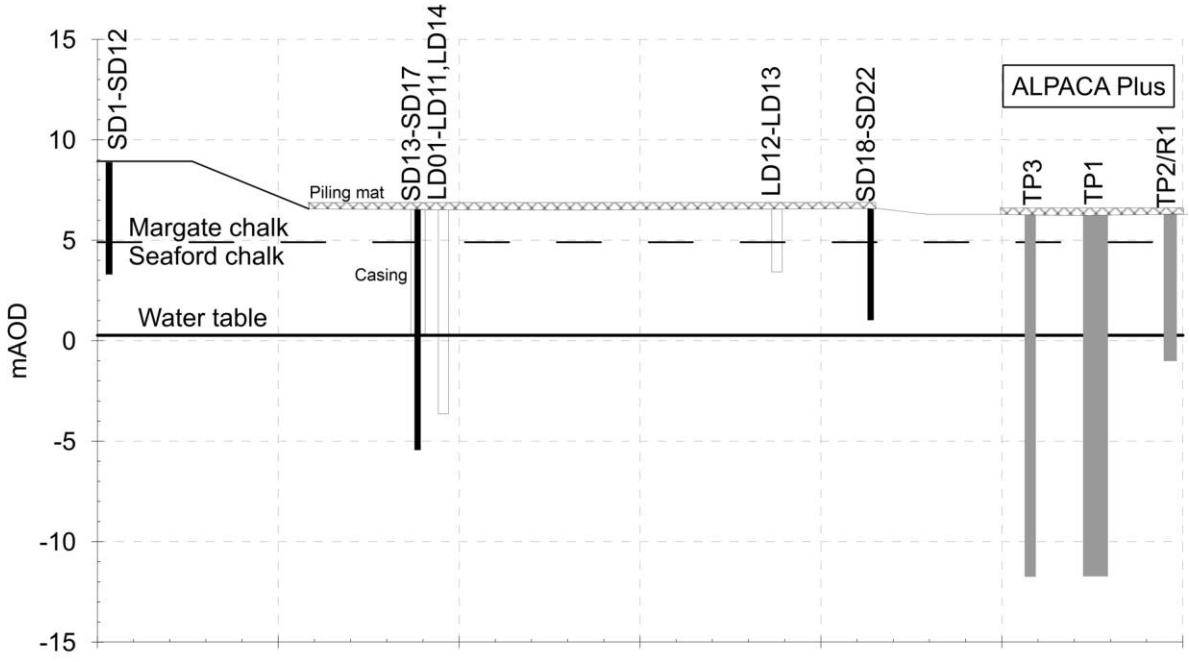

Figure 1(b)

Accepted manuscript doi:
10.1680/jgeot.22.00041

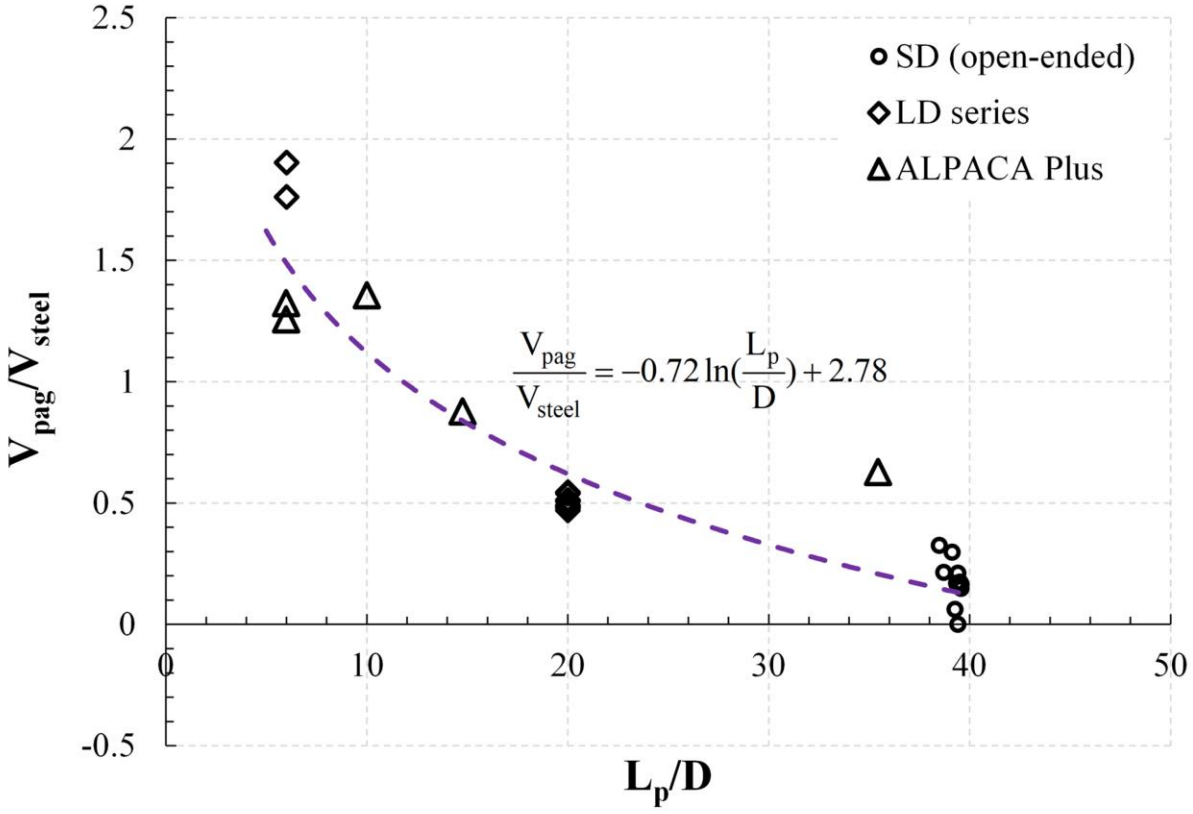

Figure 2

Accepted manuscript doi:
10.1680/jgeot.22.00041

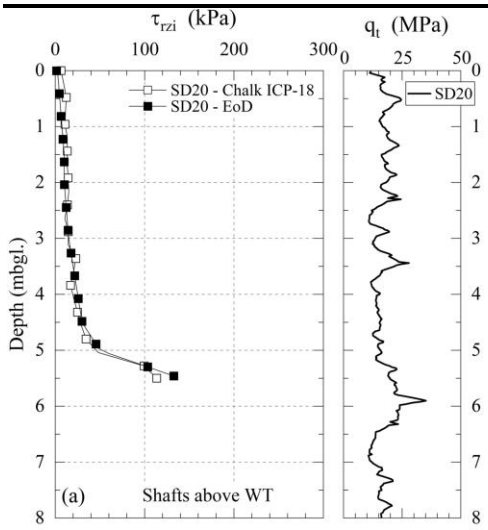

Figure 3(a)

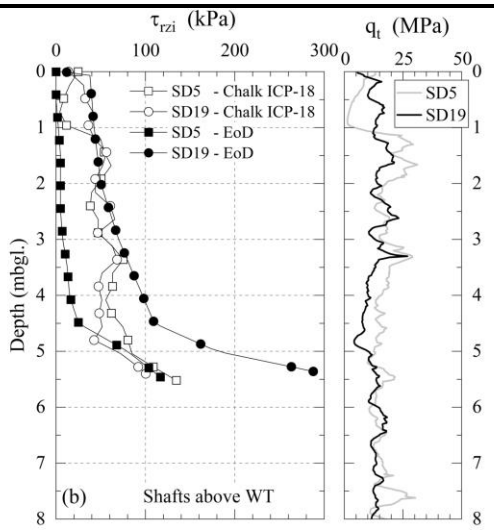

Figure 3(b)

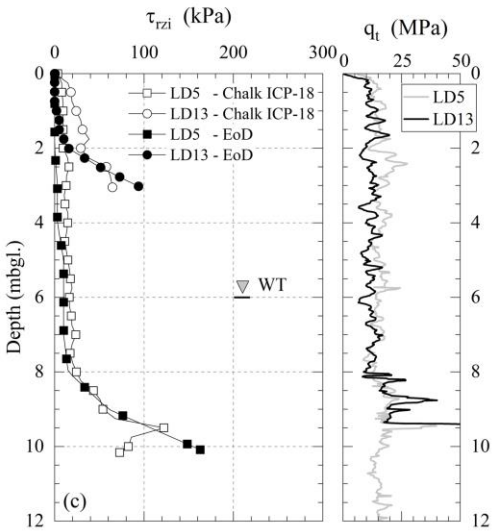

Figure 3(c)

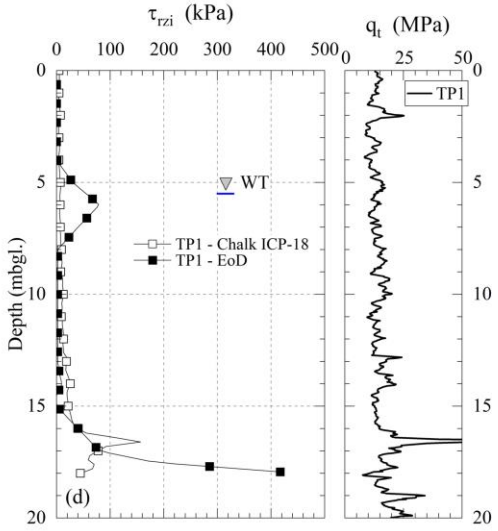

Figure 3(d)

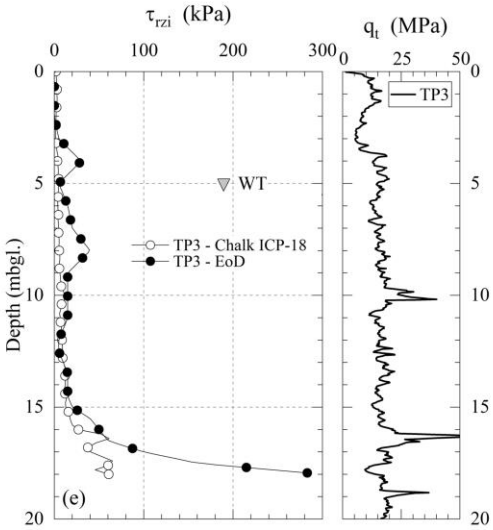

Figure 3(e)

Accepted manuscript doi:
10.1680/jgeot.22.00041

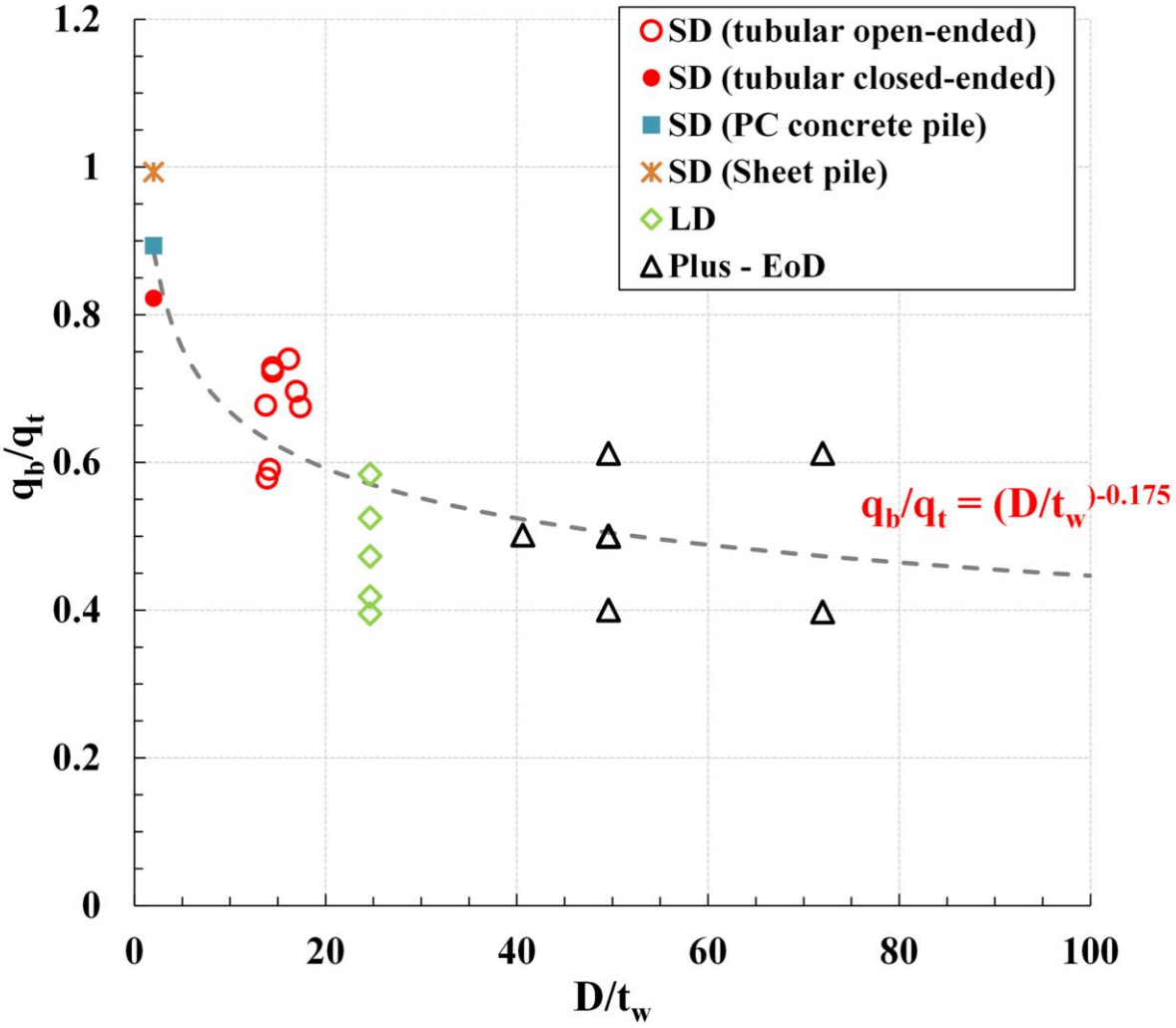

Figure 4

Accepted manuscript doi:
10.1680/jgeot.22.00041

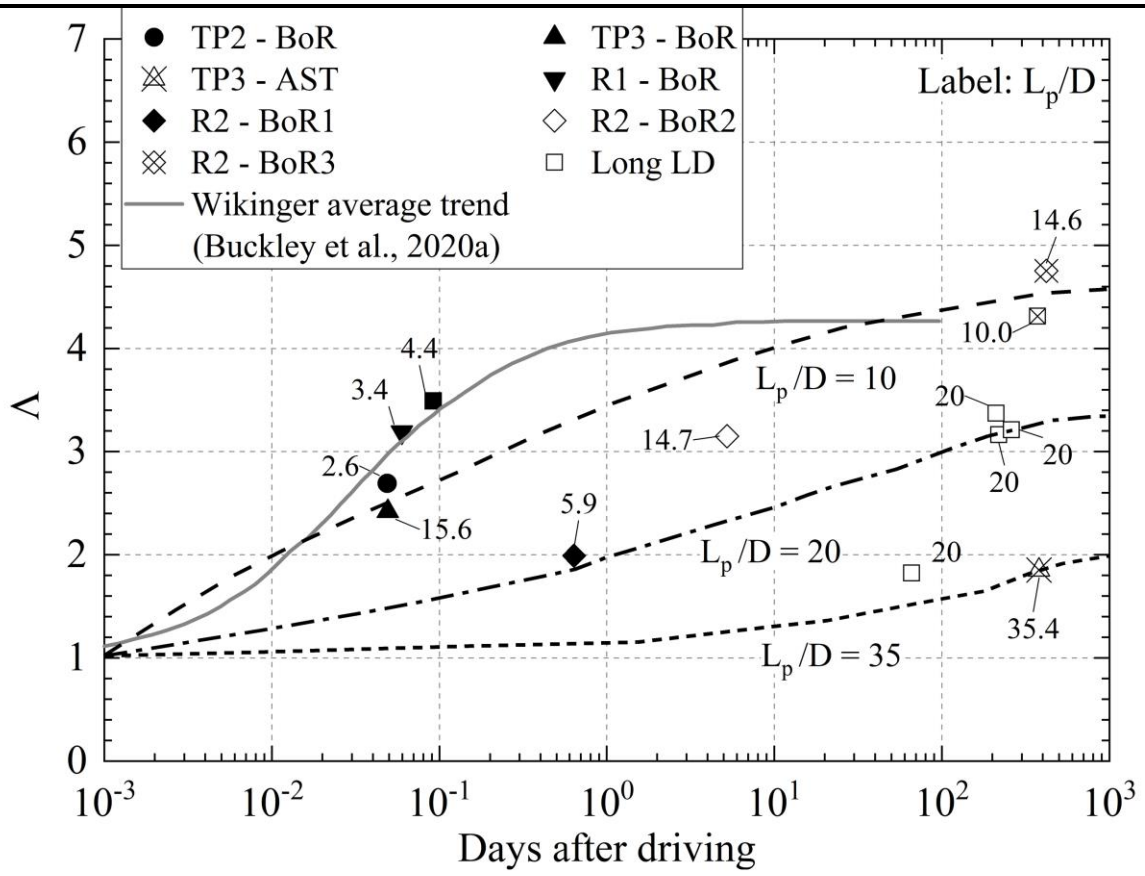

Figure 5

Accepted manuscript doi:
10.1680/jgeot.22.00041

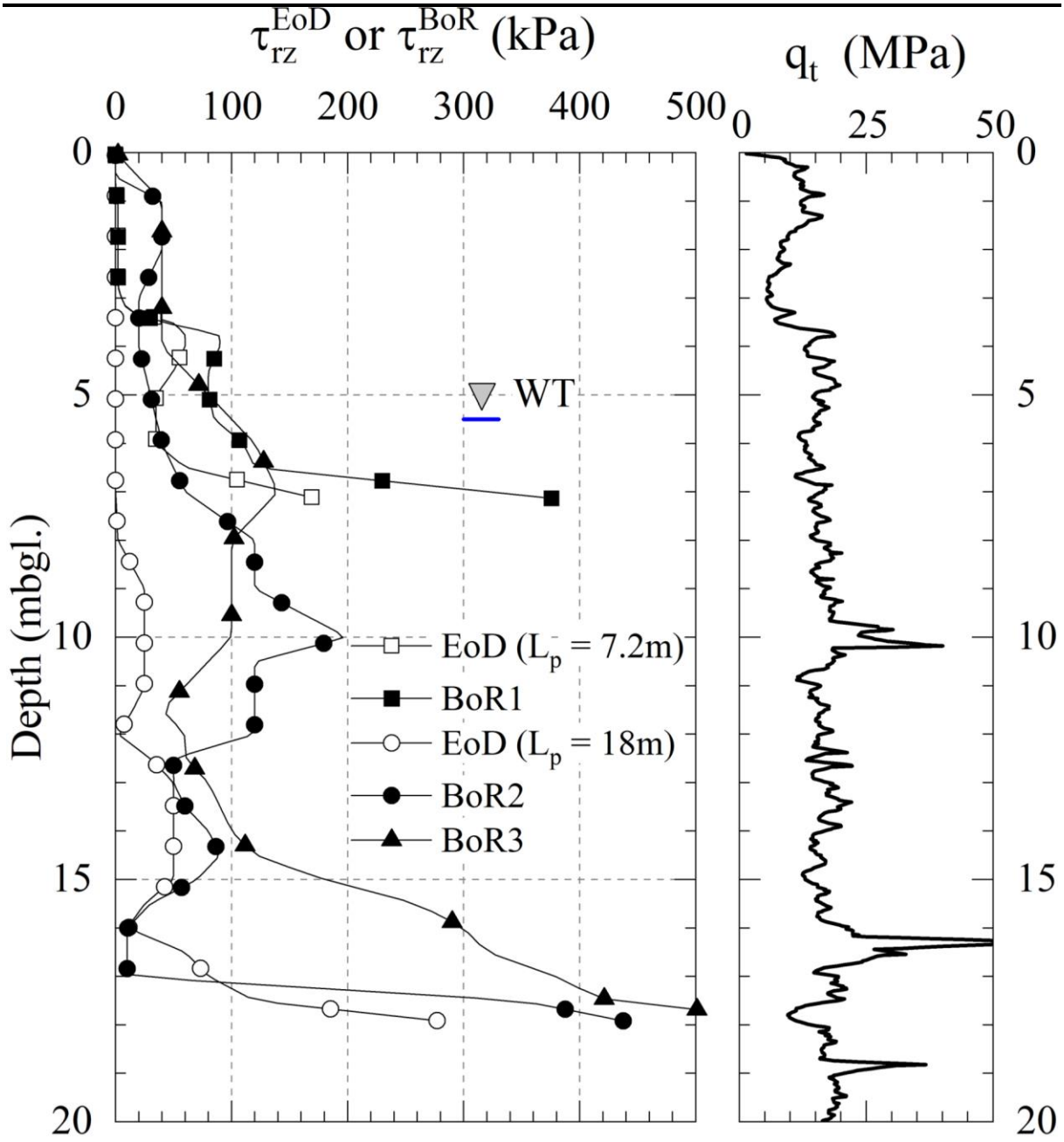

Figure 6

Accepted manuscript doi:
10.1680/jgeot.22.00041

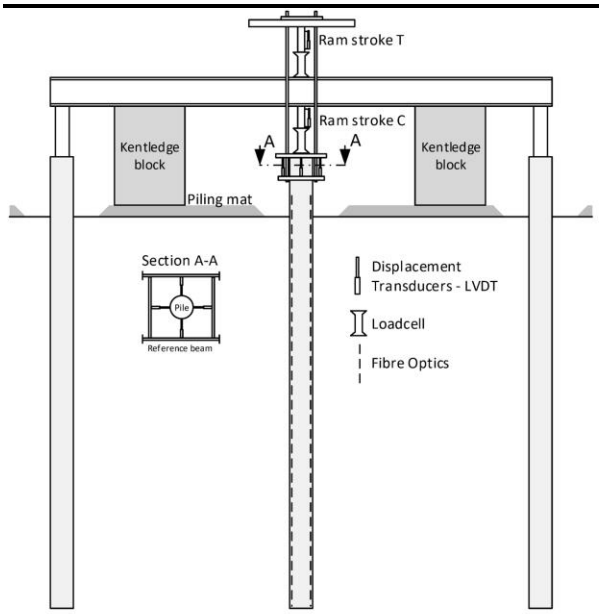

Figure 7(a)

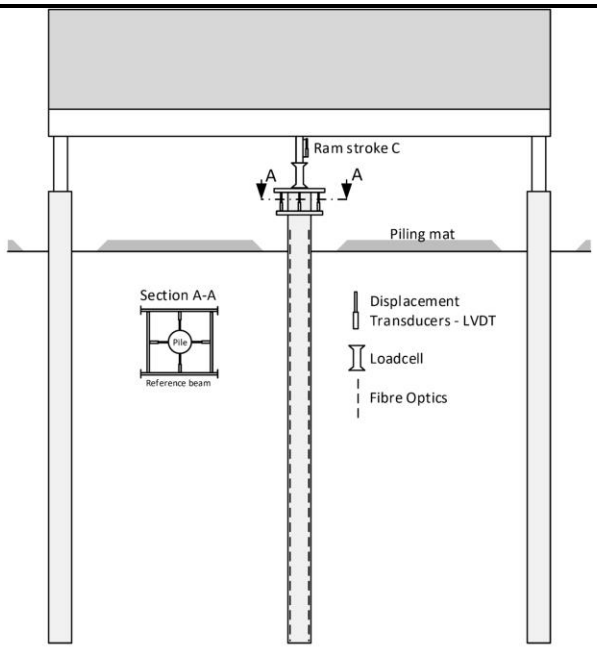

Figure 7(b)

Accepted manuscript doi:
10.1680/jgeot.22.00041

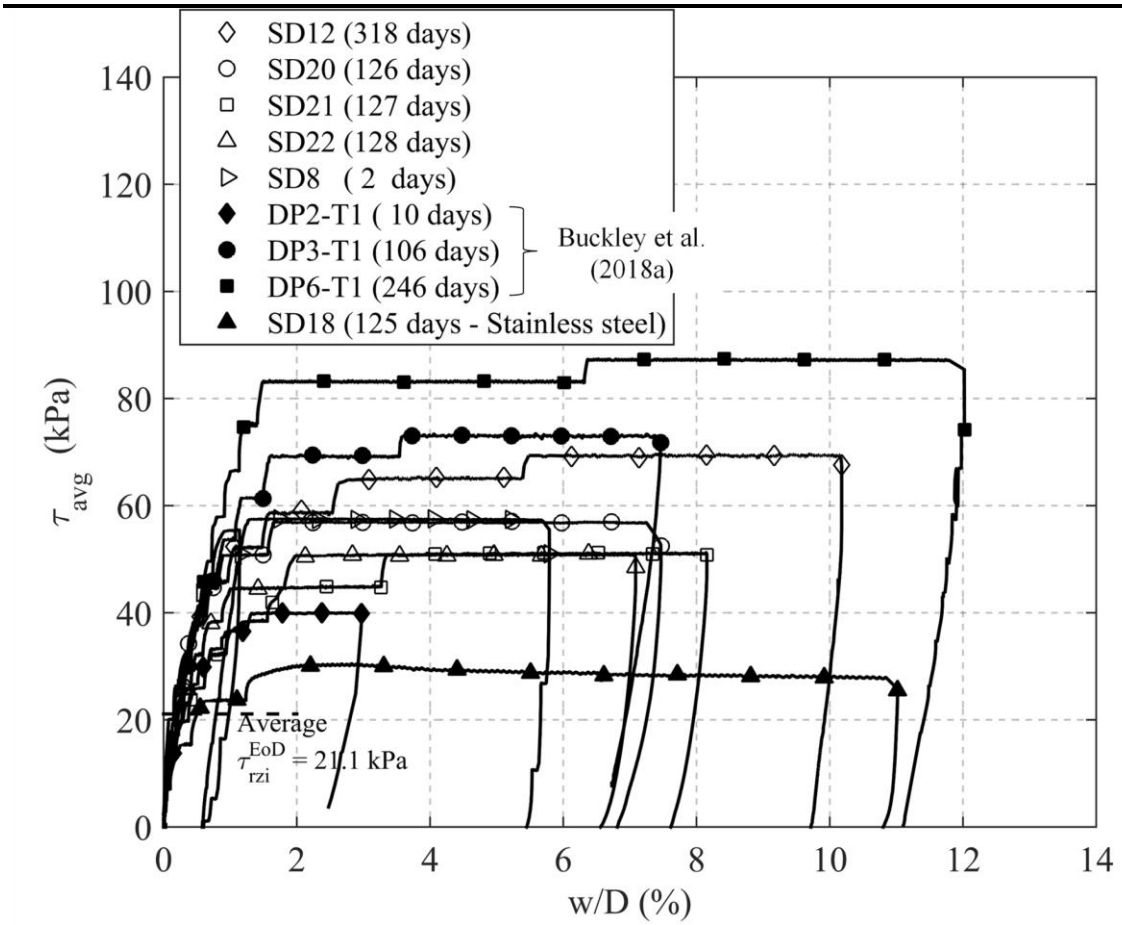

Figure 8

Accepted manuscript doi:
10.1680/jgeot.22.00041

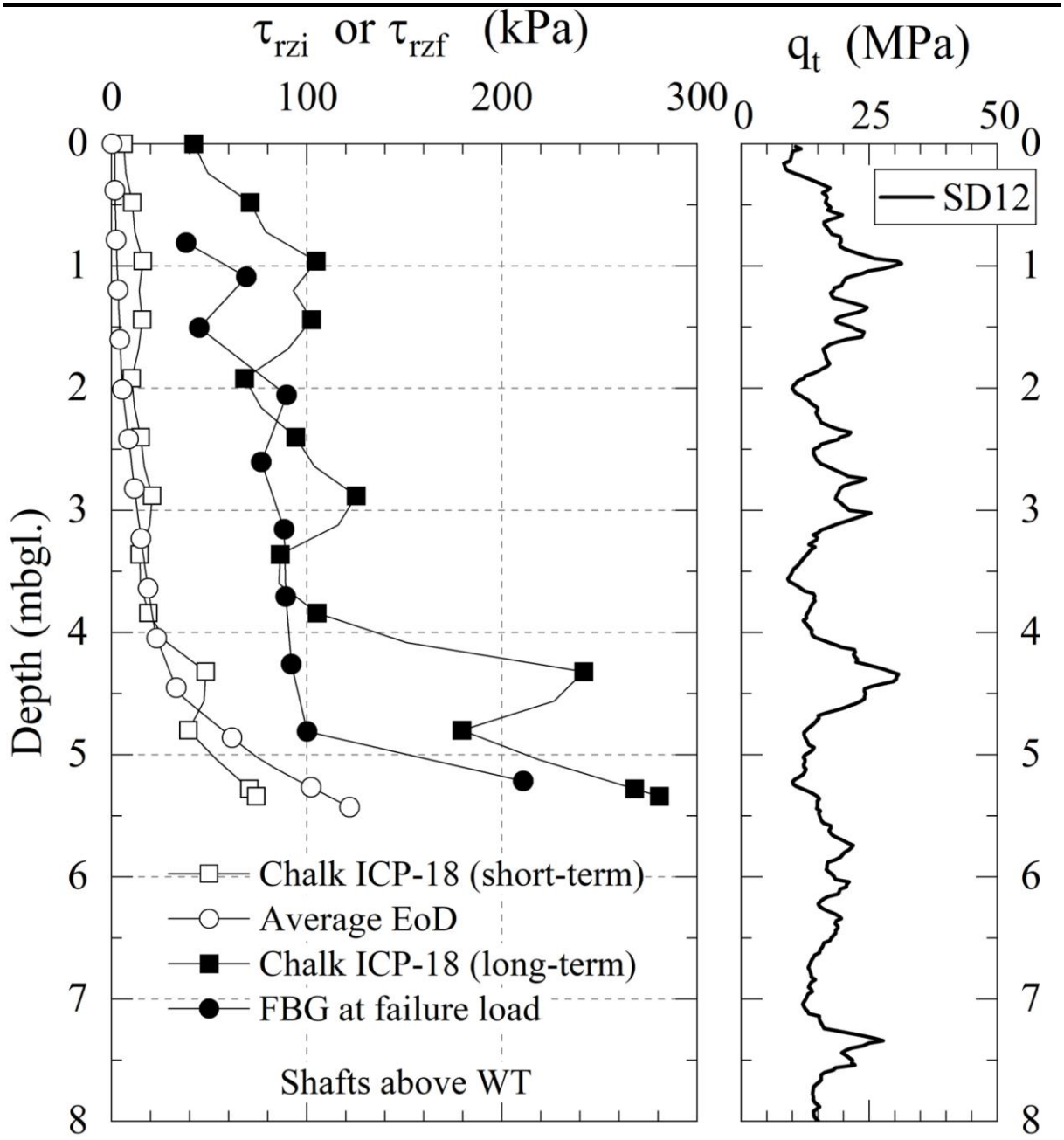

Figure 9

Accepted manuscript doi:
10.1680/jgeot.22.00041

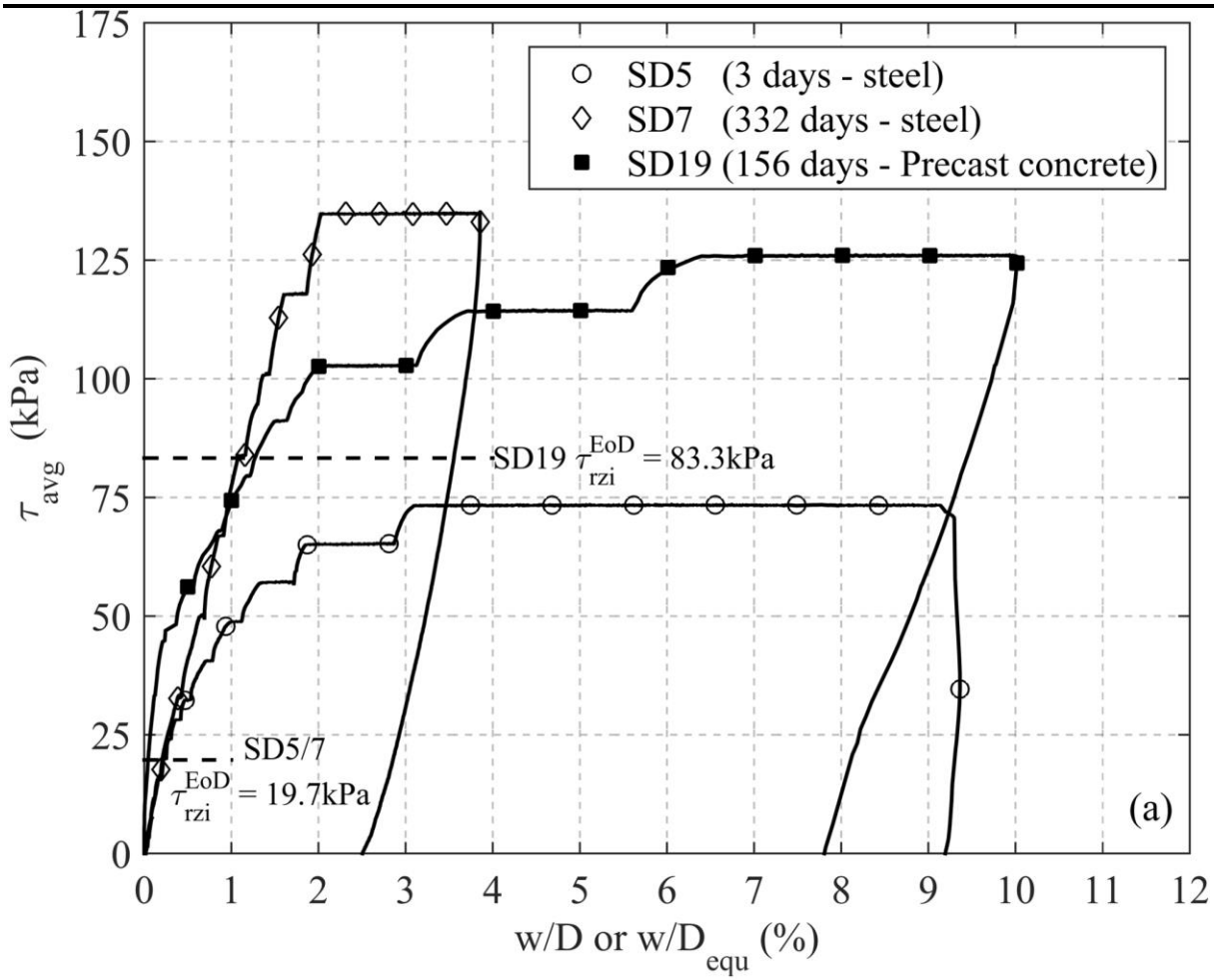

Figure 10

Accepted manuscript doi:
10.1680/jgeot.22.00041

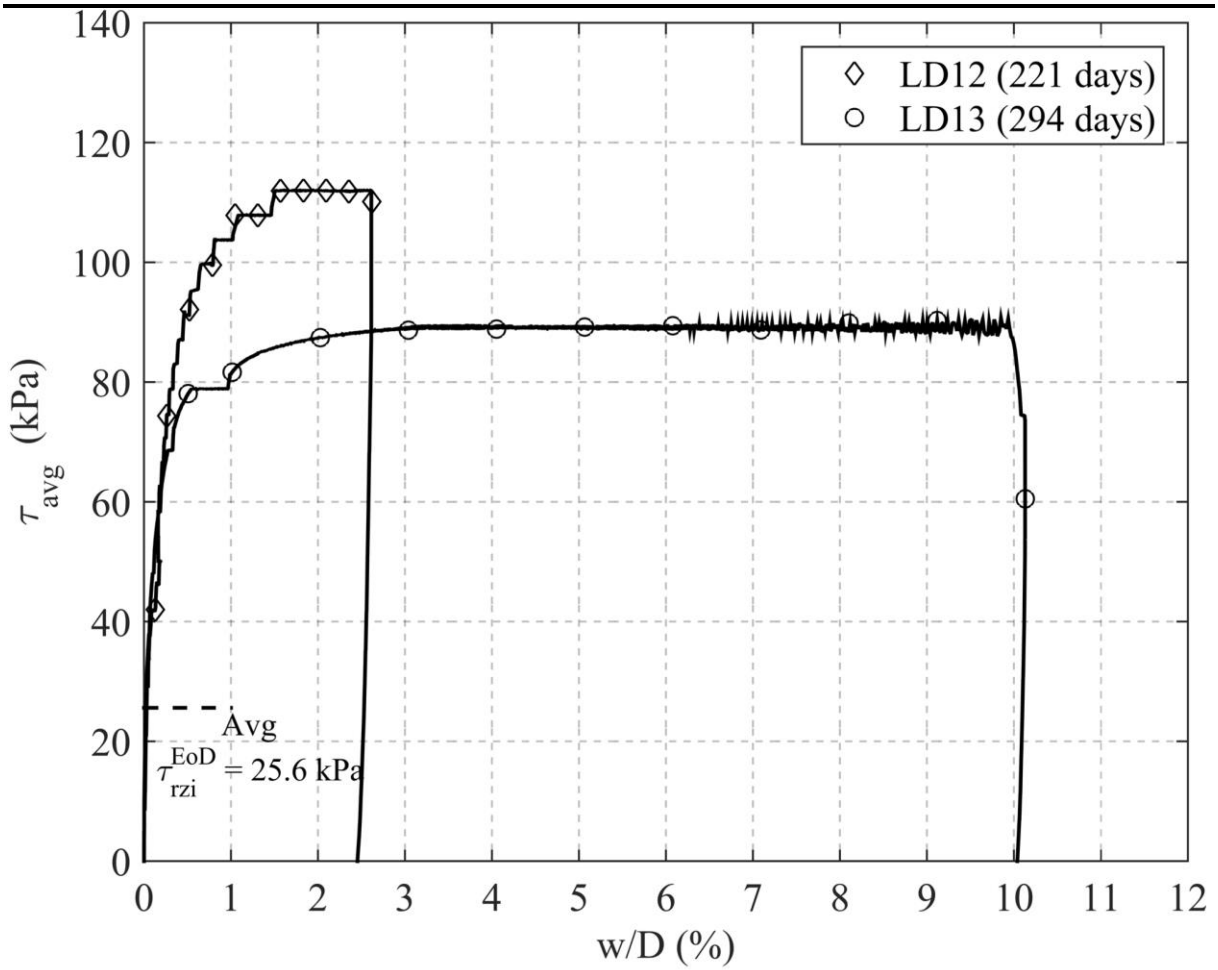

Figure 11

Accepted manuscript doi:
10.1680/jgeot.22.00041

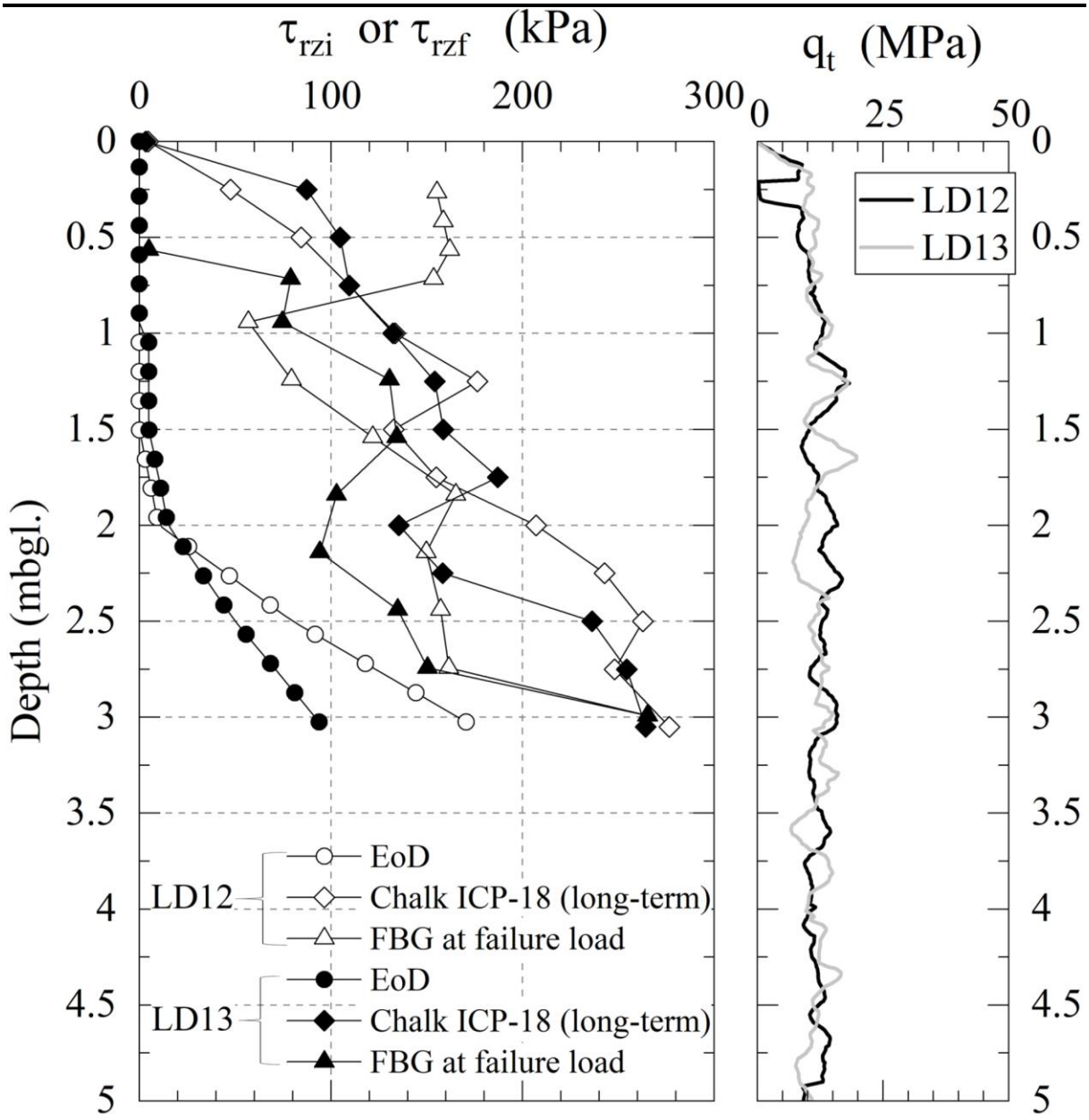

Figure 12

Accepted manuscript doi:
10.1680/jgeot.22.00041

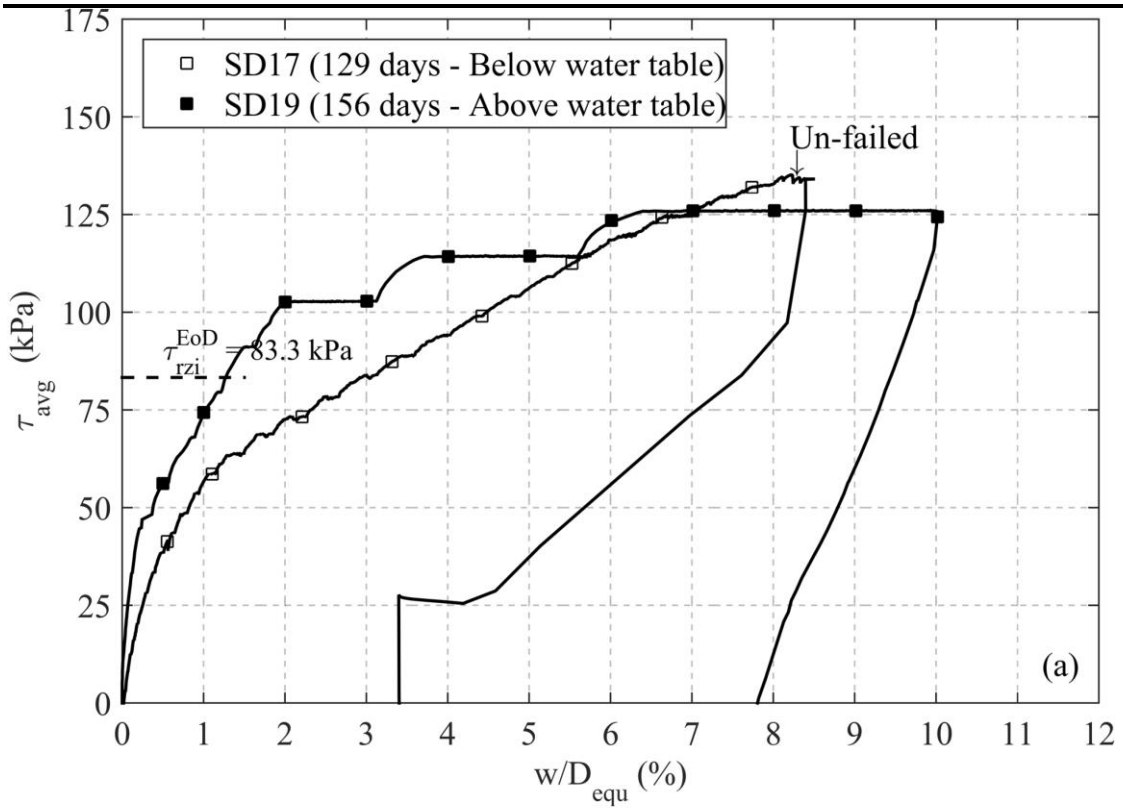

Figure 13(a)

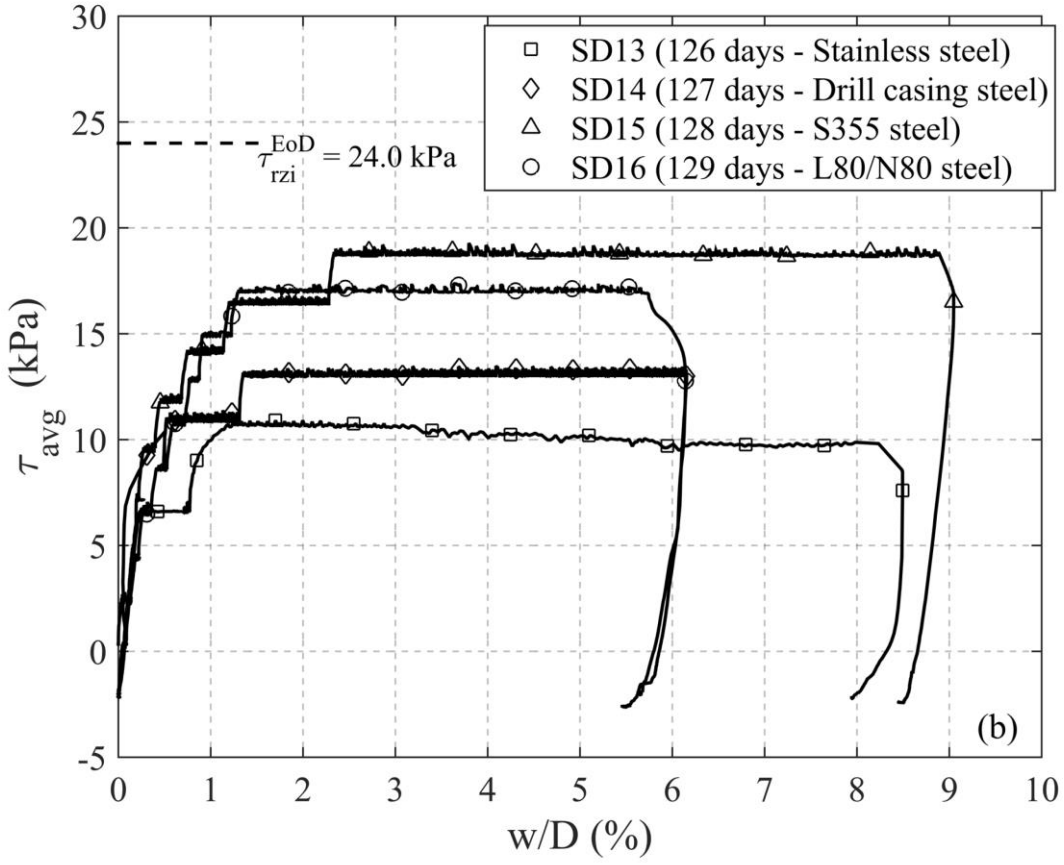

Figure 13(b)

Accepted manuscript doi:
10.1680/jgeot.22.00041

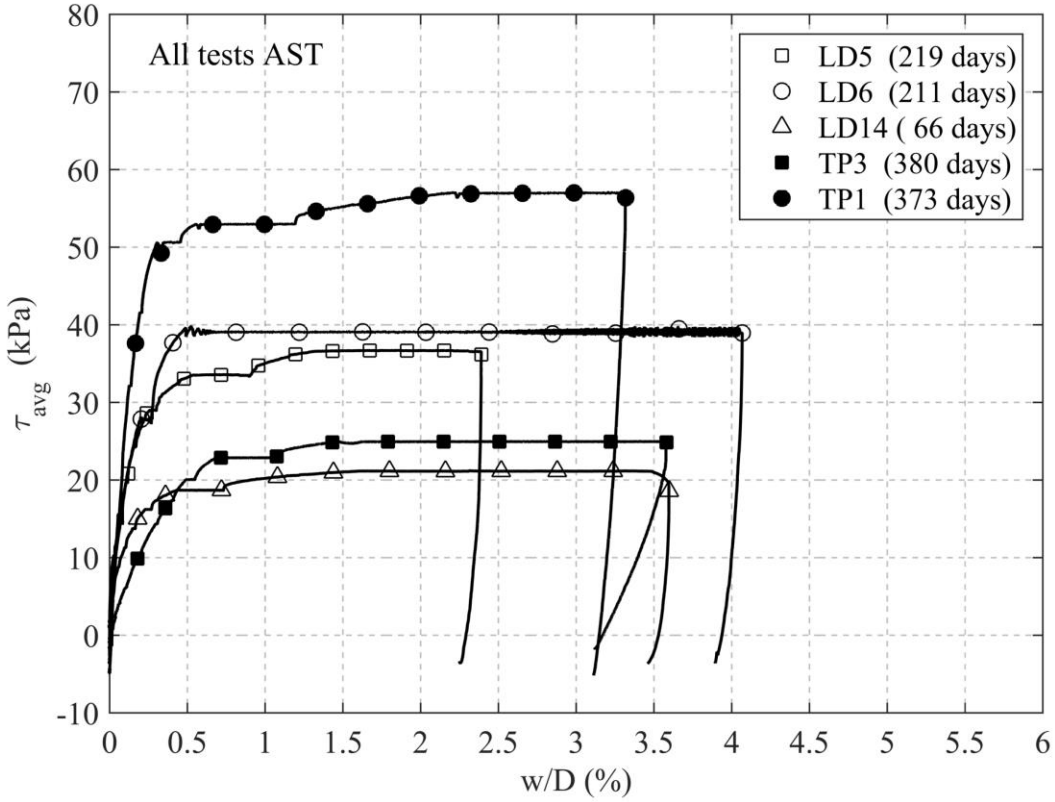

Figure 14

Accepted manuscript doi:
10.1680/jgeot.22.00041

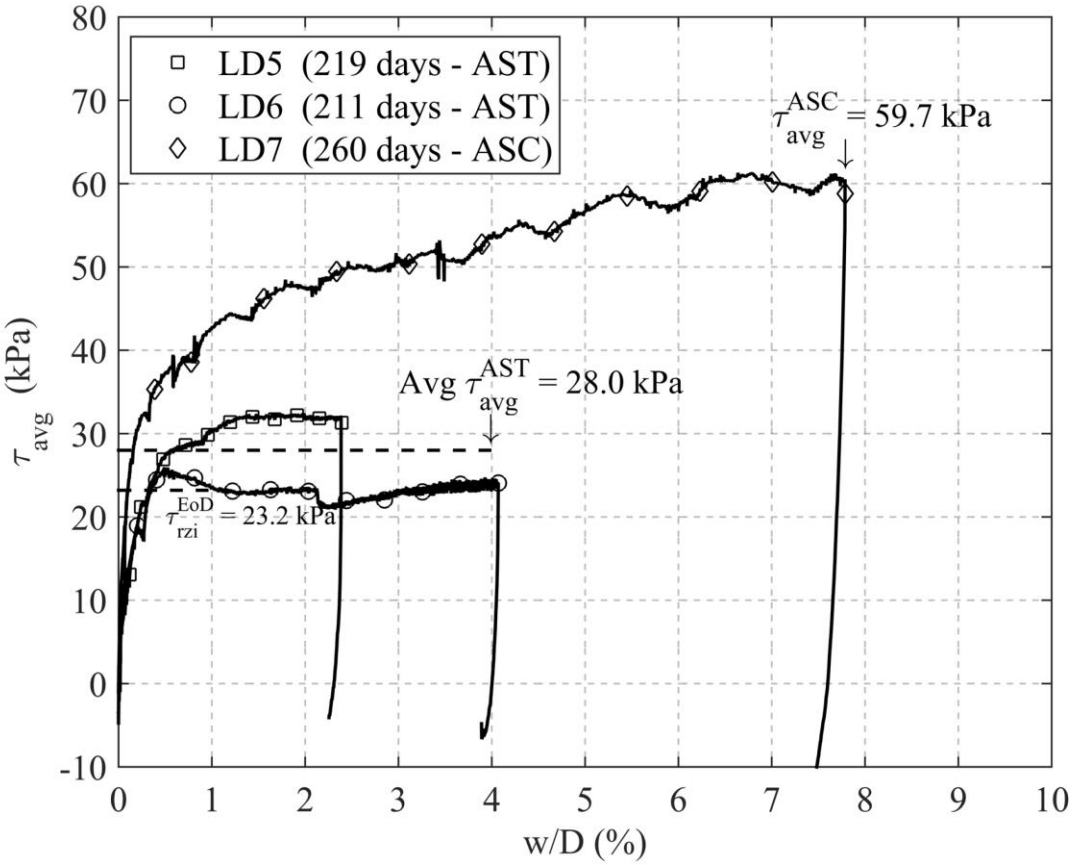

Figure 15

Accepted manuscript doi:
10.1680/jgeot.22.00041

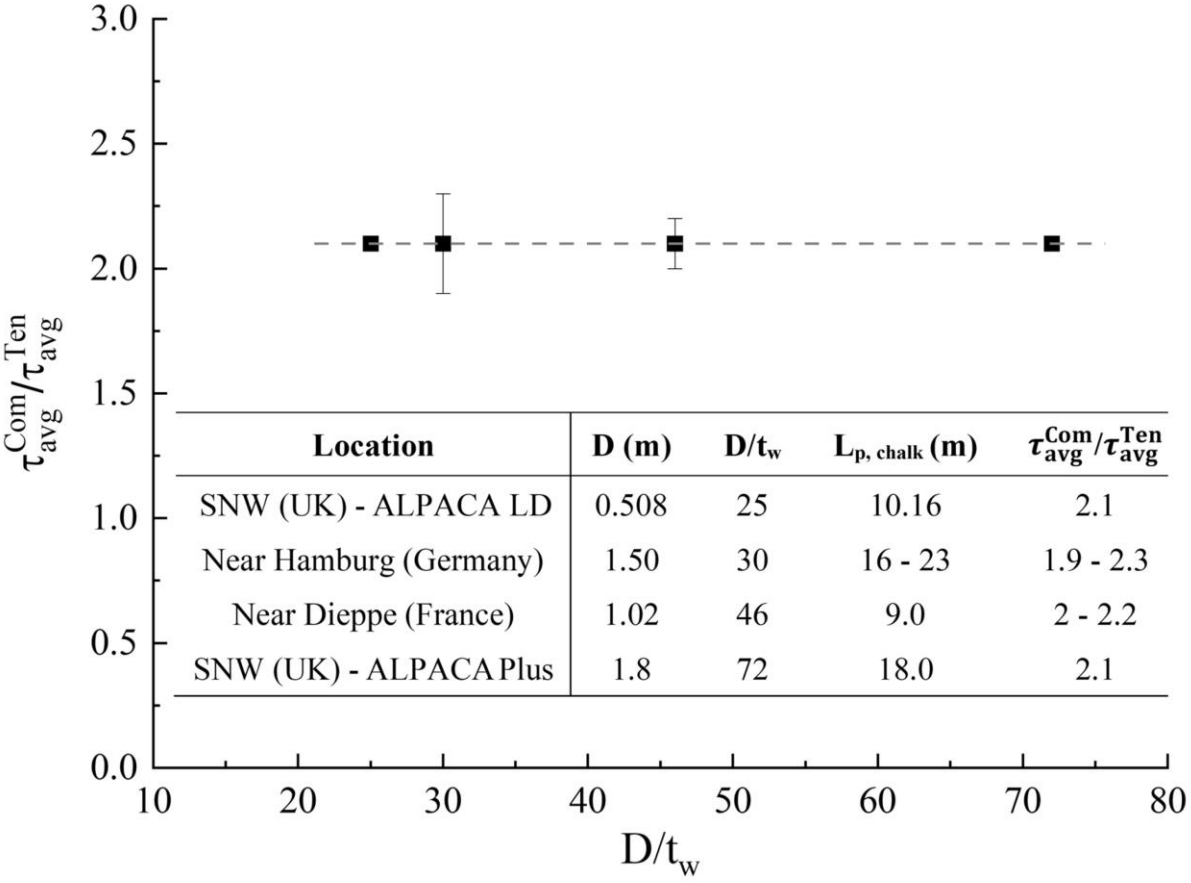

Location	D (m)	D/t_w	$L_{p,\ chalk}$ (m)	$\tau_{avg}^{Com}/\tau_{avg}^{Ten}$
SNW (UK) - ALPACA LD	0.508	25	10.16	2.1
Near Hamburg (Germany)	1.50	30	16 - 23	1.9 - 2.3
Near Dieppe (France)	1.02	46	9.0	2 - 2.2
SNW (UK) - ALPACA Plus	1.8	72	18.0	2.1

Figure 16

Accepted manuscript doi:
10.1680/jgeot.22.00041

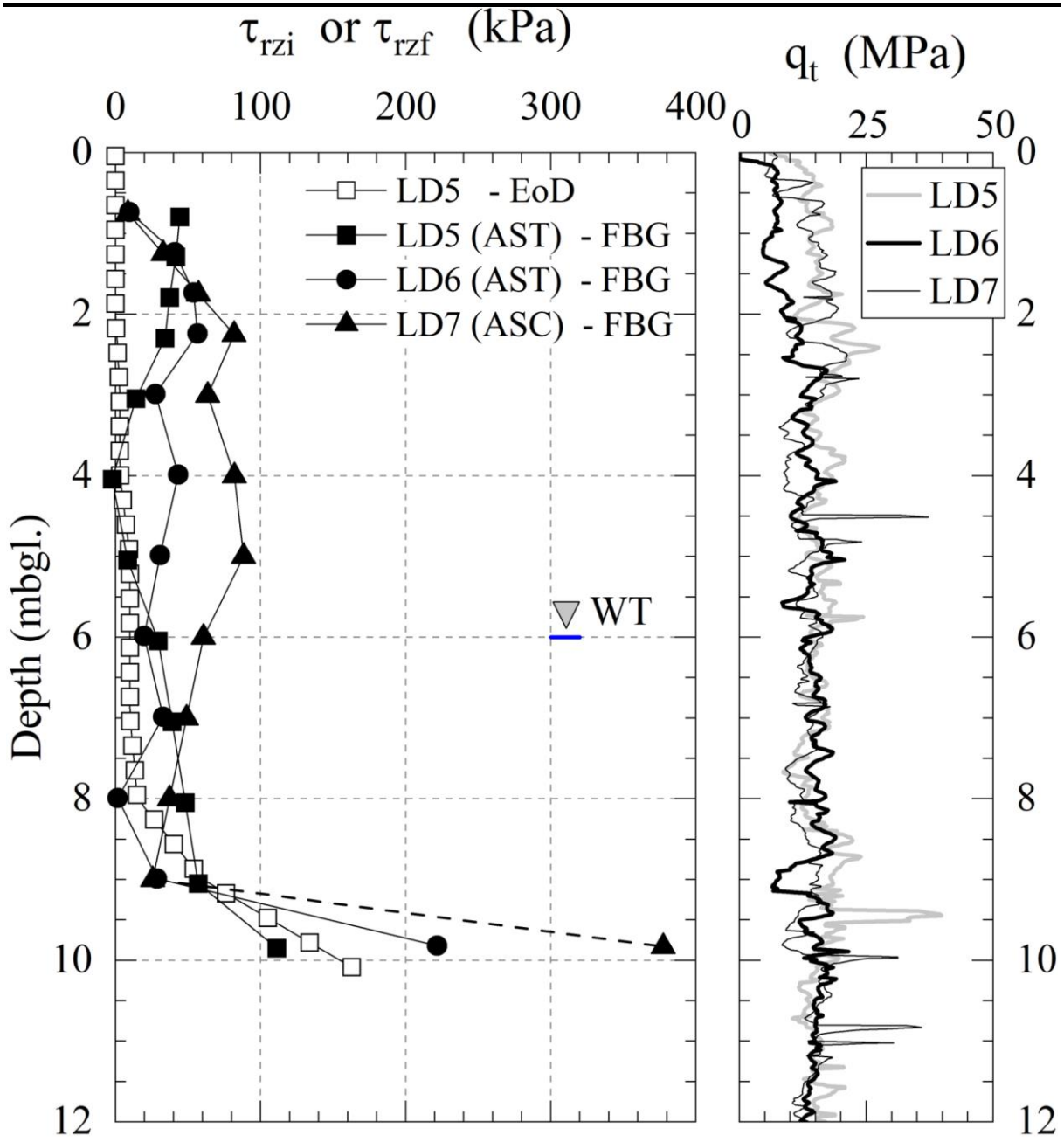

Figure 17

Accepted manuscript doi:
10.1680/jgeot.22.00041

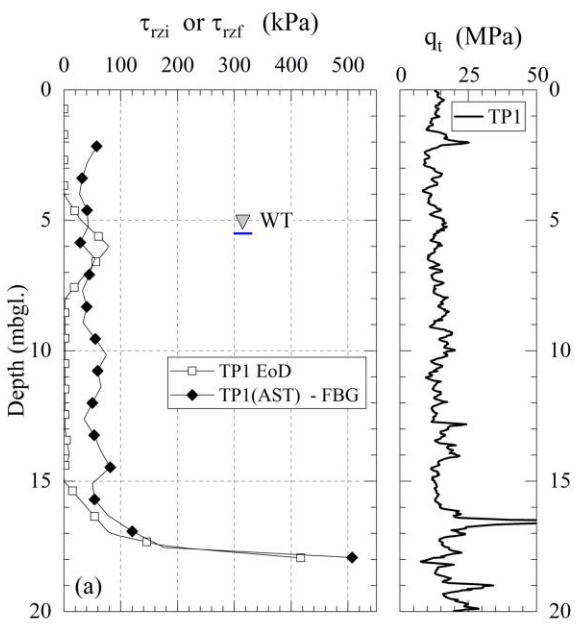

Figure 18(a)

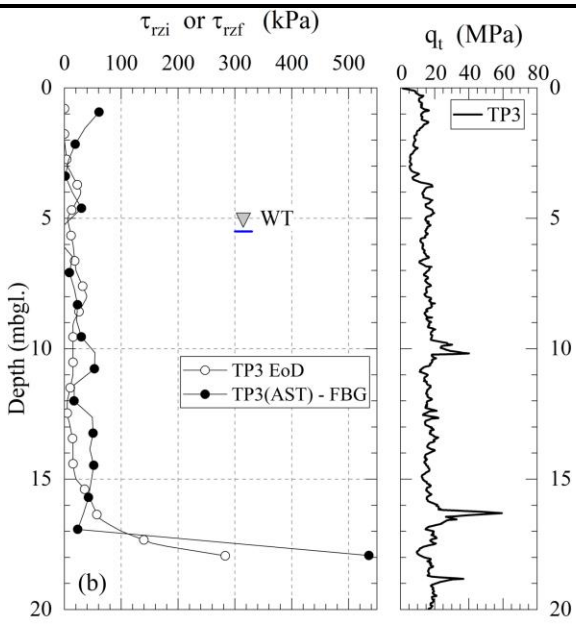

Figure 18(b)

Accepted manuscript doi:
10.1680/jgeot.22.00041

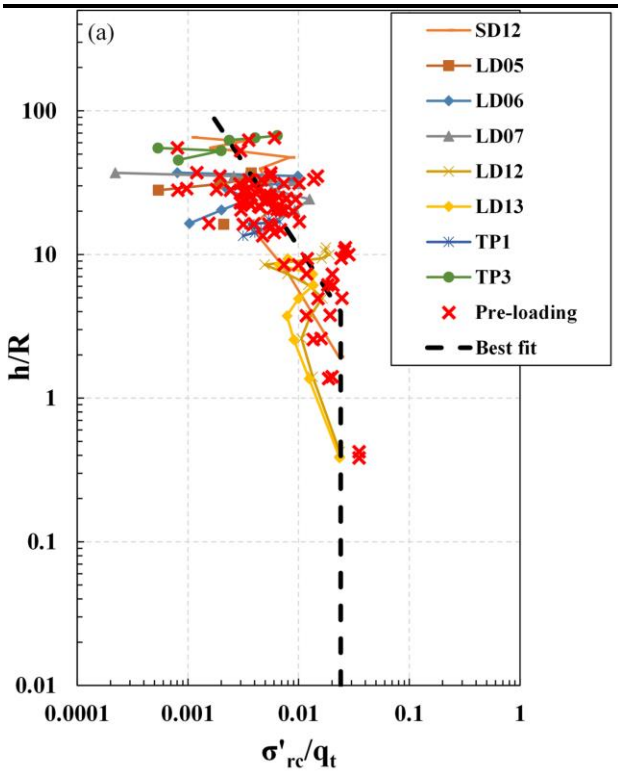

Figure 19(a)

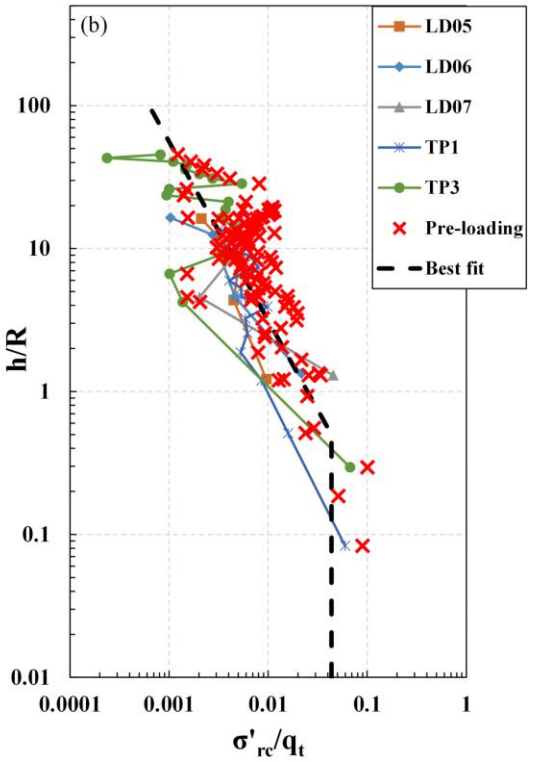

Figure 19(b)

Accepted manuscript doi:
10.1680/jgeot.22.00041

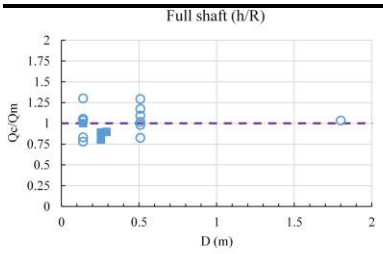

Figure 20(a)

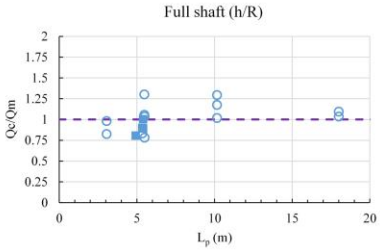

Figure 20(b)

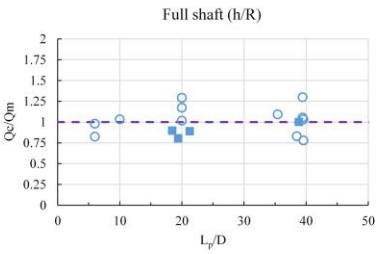

Figure 20(c)

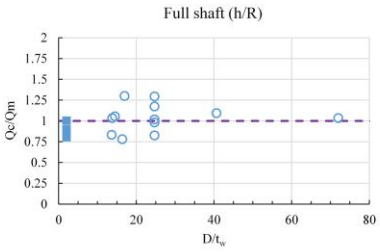

Figure 20(d)

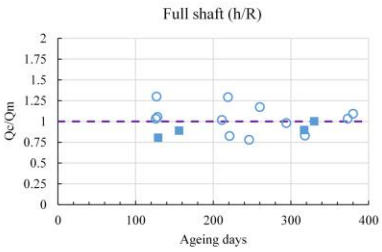

Figure 20(e)